

AD 727064

AFML-TR-71-119

GRAPHITE MELTING BEHAVIOR

N. S. Diaconis
E. R. Stover
J. Hook
G. J. Catalano

Re-Entry and Environmental Systems Division
General Electric Company

TECHNICAL REPORT AFML-TR-71-119

JULY 1971

**This document has been approved for public release
and sale; its distribution is unlimited.**

**Air Force Materials Laboratory
Air Force Systems Command
Wright-Patterson Air Force Base, Ohio**

RECEIVED
A

Reproduced by
**NATIONAL TECHNICAL
INFORMATION SERVICE**
Springfield, Va. 22151

NOTICE

When Government drawings, specifications, or other data are used for any purpose other than in connection with a definitely related Government procurement operation, the United States Government thereby incurs no responsibility nor any obligation whatsoever; and the fact that the government may have formulated, furnished, or in any way supplied the said drawings, specifications, or other data, is not to be regarded by implication or otherwise as in any manner licensing the holder or any other person or corporation, or conveying any rights or permission to manufacture, use, or sell any patented invention that may in any way be related thereto.

ACCESSION for		
CFSTI	WHITE SECTION	<input checked="" type="checkbox"/>
DDC	BUFF SECTION	<input type="checkbox"/>
UNANNOUNCED		<input type="checkbox"/>
JUSTIFICATION		
BY		
DISTRIBUTION/AVAILABILITY		
DIST.	AVAIL.	WAS OF S. LEVEL
A		

Copies of this report should not be returned unless return is required by security considerations, contractual obligations, or notice on a specific document.

GRAPHITE MELTING BEHAVIOR

N. S. Diaconis
E. R. Stover
J. Hook
G. J. Catalano

This document has been approved for public release
and sale; its distribution is unlimited.

DOCUMENT CONTROL DATA - R & D

(Security classification of title, body of abstract and indexing annotation must be entered when the overall report is classified)

1. ORIGINATING ACTIVITY (Corporate author) General Electric Company Environmental Sciences Laboratory Philadelphia, Penna. 19101		2a. REPORT SECURITY CLASSIFICATION Unclassified	
3. REPORT TITLE GRAPHITE MELTING BEHAVIOR		2b. GROUP	
4. DESCRIPTIVE NOTES (Type of report and inclusive dates) Final Report (July 1968 to June 1970)			
5. AUTHOR(S) (First name, middle initial, last name) N.S. Diaconis J. Hook E. R. Stover G.J. Catalano			
6. REPORT DATE July 1971	7a. TOTAL NO. OF PA 72	7b. NO. OF REFS 18	
8a. CONTRACT OR GRANT NO. F33315-68-C-1713	9a. ORIGINATOR'S REPORT NUMBER(S) AFML-TR-71-119		
b. PROJECT NO. 7350	9b. OTHER REPORT NO(S) (Any other numbers that may be assigned this report)		
c. Task No 735002			
10. DISTRIBUTION STATEMENT This document has been approved for public release and sale; its distribution is unlimited.			
11. SUPPLEMENTARY NOTES		12. SPONSORING MILITARY ACTIVITY Metals and Ceramics Division Air Force Materials Laboratory Wright-Patterson Air Force Base, Ohio	
13. ABSTRACT An experimental program was conducted to determine the melting behavior of graphite. Data was obtained with an electric arc heater, and a resistance heater over a pressure range from the triple point to approximately 320 atmospheres. Temperature measurements were made in the arc heater environment with a scanning spectrometer while a recording optical pyrometer was used for the resistively heated specimens. ATJS and pyrolytic graphite were the test materials and argon and nitrogen were the test gases. Within the accuracy of the data the results did not show any discernible difference with gas environments. Arc heater data showed a slight increase in melting temperature over that exhibited by the resistively heated models. Values for the triple point were determined to be 102 atmospheres pressure with temperatures varying between 4100°K and 4300°K depending upon mode of heating and material.			

Unclassified

Security Classification

14. KEY WORDS	LINK A		LINK B		LINK C	
	ROLE	WT	ROLE	WT	ROLE	WT
Graphite Phase Diagram Triple Point Melting Point Microstructure Radiation Heating Resistance Heating Electric Arc Heating						

Unclassified

Security Classification

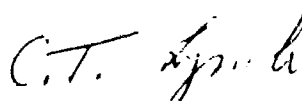
FORWORD

This report was prepared by the Re-Entry and Environmental Systems Division of the General Electric Company under USAF Contract No. F33615-68-C-1713. The contract was initiated under Project 7350, "Refractory, Inorganic Nonmetallic Materials," Task No. 735002, "Refractory, Inorganic Nonmetallic Materials: Graphitic." The work was administered by the Air Force Materials Laboratory, Wright-Patterson Air Force Base, Ohio with Dr. L.R. Bidwell (AFML/LLS), Project Scientist.

The time period of the contract was from July 1968 to June 1970. The report was submitted by the authors in February 1971.

The authors wish to acknowledge Dr. C.H. Marston, Mr. N.M. Jaffe, Mr. J.R. Mallin, and Mr. J.P. Brazel for their assistance in acquiring and evaluating the temperature data. The support of Mr. F.P. Magin and Mr. W. Staley in obtaining and analyzing the microstructure photographs is greatly appreciated. The effort of Mr. D.A. Rogers and Mr. W. Brandkamp in support of the laser experiments is also acknowledged. The exceptional logistical support provided by Mr. R. Bendorovich without whose help the experiments could not have been conducted and the encouragement by Mr. M.J. Engel is duly recognized. Finally, the authors wish to thank Dr. P.D. Zavitsanos for the stimulating discussions and his counsel throughout the program.

This technical report has been reviewed and is approved.



C. T. LYNCH
Chief, Advanced Metallurgical
Studies Branch
Metals and Ceramics Division
Air Force Materials Laboratory

ABSTRACT

An experimental program was conducted to determine the melting behavior of graphite. Data was obtained with an electric arc heater, and a resistance heater over a pressure range from the triple point to approximately 320 atmospheres. Temperature measurements were made in the arc heater environment with a scanning spectrometer while a recording optical pyrometer was used for the resistively heated specimens. ATJS and pyrolytic graphite were the test materials and argon and nitrogen were the test gases. Within the accuracy of the data the results did not show any discernible difference with gas environments. Arc heater data showed a slight increase in melting temperature over that exhibited by the resistively heated models. Values for the triple point were determined to be 102 atmospheres pressure with temperatures varying between 4100°K and 4300°K depending upon mode of heating and material.

TABLE OF CONTENTS

Section	Page
I. INTRODUCTION	1
II. EXPERIMENTAL APPROACH	3
A. Heating Techniques	3
B. Test Materials	3
C. Instrumentation	4
III. SPECIMEN HEATING BY ELECTRIC ARC	5
A. Arc Radiation Heating	5
B. Arc Radiation and Ohmic Heating	7
IV. RESISTIVE HEATING OF SPECIMENS	9
V. SPECIMEN HEATING BY LASER	11
A. Laser Facility Preparation	11
B. Laser Pulse Broadening	12
C. Specimen Tests	13
VI. SURFACE TEMPERATURE MEASUREMENT	14
A. Description of Scanning Spectrometer	14
B. Spectrometer Optics	15
C. Temperature from Spectrometer Data	15
D. Analysis of Spectrometer Signal Interpretation	16
E. Spectrometer Wavelength Calibration	18
VII. RESULTS AND DISCUSSION	20
A. Arc Heating	20
B. Resistance Heating	21
C. Laser Heating	24
D. Microstructure of Solidified Graphite	25
E. Phase Diagram	26
F. Concluding Remarks	30
VIII. REFERENCES	32

LIST OF ILLUSTRATIONS

FIGURE		PAGE
1a	High Pressure Arc, MK II	34
1b	Test Arrangement for Arc Heating of Graphite Specimens	35
2	Pulsed Laser Used for Specimen Heating	36
3a	Resistive Heater Assembly	37
3b	Resistive Heating Experimental Apparatus	38
4	Sketch of MK II Arc Heater Electrode Arrangement	39
5	Arc Column Radiant Intensity at 100 Atmospheres Pressure	40
6	Gas Inlet Tube Adapter for Arc Heater	41
7	Modified Electrode Arrangement for Arc Heater	42
8	Arc Heated Pyrolytic Graphite Specimen Showing Solidified Nodules on Surface at 7X and 149 ATM in Argon	43
9	Final Test Specimen Arrangement - Arc Heater	44
10	Temperature Distribution in ATJ Specimen	45
11	Spectrometer Analogue Detector Outputs	46
12	Arc Heated Pyrolytic Graphite Specimen After Test Showing Recession of Front Surface Through to Back Surface at 2X and 153 ATM in Nitrogen	47
13	Ballast Resistor for Resistance Heater	48
14	Resistance Heater Specimen Configurations	49
15	Sectioned ATJ-S Specimen After Resistance Heating Showing Solidified Interior and Expanded Cross Section at 5.5X and 135 ATM in Argon	50

LIST OF ILLUSTRATIONS (CONTINUED)

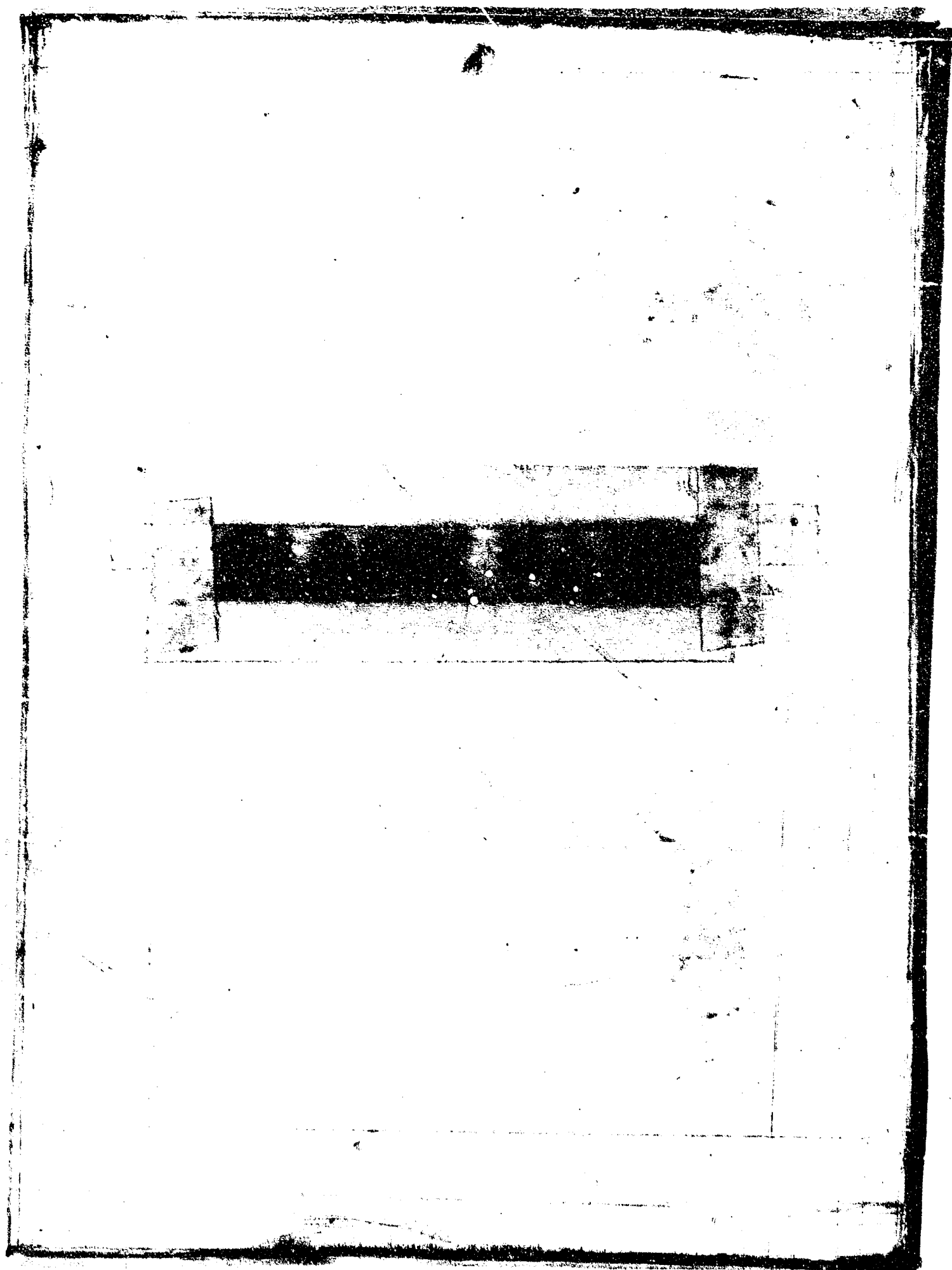
FIGURE		PAGE
16	Typical Resistance Heated Specimen After Test Showing Solidified Graphite, at 5.5X, P = 238 Atm	51
17	Short and Long Wavelength Spectrometer Scans (Black Body at 1273° K)	52
18	ATJ-S Specimens Heated in Nitrogen Environment in Arc Heater, P = 164 & 144 Atm (3.3X)	53
19	Pyrolytic Graphite Specimen Heated in Nitrogen Environment in Arc Heater, P = 164 Atm (3.3X)	54
20	Polished Section of Drop Collected from Graphite Sample Resistance Heated to High Pressure, Showing "Collapsed" Form and Crystals in the Vicinity of the Buckled Side; Left: 30X; Right, 100X. P = 203 Atm, Nitrogen Gas	55
21	Crystals in Solidified Drop Shown in Figure 20, Photographed at 860 X with Oil Immersion Lens in Polarized Light; Top: Two Regions Near Surface of Drop; Bottom: Regions from Center of Drop Showing Differences in Crystal Size	56
22	Section Through Wall of ATJ-S Resistively Heated at 238 Atm; 50 X in Polarized Light.	57
23	Views of Figure 22 at 860 X in Polarized Light, Showing Top of Left (Outer) Wall, at Top, and section Through Inner Wall with Thick Layer of Vapor Deposit, at Right.	58
24	View of Figure 22 at 860 X in Polarized Light, Showing Graphite Crystals Oriented Parallel to the Surface of the Collapsed, Solidified Drop.	59

LIST OF ILLUSTRATIONS (CONTINUED)

FIGURE		PAGE
25a	View of Figure 22 at 860 X in Polarized Light, Showing Unmelted ATJ-S, at Left, and Columnar Grains which grew from the Solid into the Liquid During Solidification.	60
25b	Continuation of Figure 25a, 860 X in Polarized Light, Showing Interface Between Columnar Solidified Material, at Left, and Crystals Solidified from Remainder of the Liquid to Surface of Drop at Right.	61
26	Arc-Heated Pyrolytic Graphite Showing Droplet Formed at 157 Atm; Left: 100 X; Right: 860 X.	62
27	Arc-Heated ATJ-S Showing Droplet Formed at 167 Atm, at 500 X (Argon Gas)	62
28	Appearance of Graphite Crystals on the Surface (Left) and Within a Graphite Droplet (Right) as Shown by Scanning Electron Microscopy. 2000 X.	63
29	Stereoscopic Views of a Graphite Droplet Showing Surface Orientation of Graphite Crystals Top: 20 X; Bottom: 500 X.	64
30	Stereoscopic Views of Same Graphite Drop Shown in Figure 29 After Sectioning with a Blade: Top: 20 X; Bottom: 500 X.	65
31	Graphite Phase Diagram.	66
32a	Emissivity Factors for Scanning Spectrometer Data	67
32b	Emissivity Factors for Scanning Spectrometer Data	68
33	Corrected Graphite Phase Diagram	69

LIST OF TABLES

<u>TABLE</u>		<u>Page</u>
I	Chemical Analyses of Graphite Materials	70
II	Test Data - Arc Heating	71
III	Test Data - Resistance Heating	72



SECTION I

INTRODUCTION

The use of graphite to withstand the extreme thermal environments encountered by advanced re-entry vehicles appears to be an attractive solution to a most pressing problem area. Considerable data has been generated on graphite performance at elevated temperatures both in the laboratory and from experimental flight programs. Because of the severity of the flight environments however it has not been possible to simulate properly in laboratory studies all the key flight parameters so as to obtain a good indication of expected flight performance and thereby assure successful re-entry. Faced with these conditions the designer is forced to rely on theoretical analyses to predict expected performance in these severe environments. To obtain credible predictions of course requires an accurate knowledge of material properties; much data has been collected but more is required. The objective of the study reported herein has been to explore more fully the onset of graphite melting at high temperature and pressure, - the occurrence of the triple point and the location of the solid-liquid boundary on the phase diagram.

The melting of carbon has been a subject of investigation by scientists for a number of years. In 1939 Bassat⁽¹⁾ reported an extensive series of experiments in which he heated carbon rods in an atmosphere of high pressure argon. By use of an optical pyrometer for temperature measurement and by careful observation of the character of the rod after the experiment, he established the graphite-liquid-vapor triple point to be near 100 atmospheres pressure and 4000°K (7200°R). Later Steinle⁽²⁾, Jones⁽³⁾, Noda⁽⁴⁾, Fateeva⁽⁵⁾, and Schoessow⁽⁶⁾ conducted investigations in which the triple point was indicated to occur between 100 and 140 atmospheres pressure and temperatures in the range of 3670 to 4020°K . Jones⁽³⁾ used an argon pressure chamber and an electrically insulated guard heater ring around the test specimen. Temperature measurements were made by observing the surface within a black body cavity drilled into the specimen material. Measurements of temperature were made until electrical failure. Noda⁽⁴⁾ performed similar experiments with small specimens also using specimen failure to establish the onset of melt. Fateeva⁽⁵⁾ used extremely small specimens (~ 1 mm diameter) and heated them until failure. Temperature measurement was by two-color pyrometer observations into a black body cavity. Provision was also made for pressure relief of vapor generation from within the specimen diameter. Onset of melt was determined by the variation of the measured electrical resistance of the specimen with electrical power applied.

Extrapolated vapor pressure data (7) (8) (9) on the other hand, at temperatures near the previously accepted triple point temperature region of 4000°K (7200°R) indicate the vapor pressure to be on the order of one atmosphere. To

achieve vapor pressure values of 100 atmospheres for the triple point would require surface temperatures on the order of 5000°K (9000°R) based on extrapolations of these lower pressure data. These uncertainties in the solid-liquid-vapor boundaries were the motivation for the present study.

In an attempt to resolve the apparent impasse presented by the different data, the graphite melting phenomenon was explored by employing more than a single heating technique. These investigations were aimed at eliminating some of the variables, thus increasing the probability of compatibility between one technique and another. The specific objective of the present study was to produce externally heated melted specimens and compare the results with data obtained using the electrical resistance heating technique. The work was conducted in the Environmental Sciences Laboratory of the General Electric Re-Entry and Environmental Systems Division under the sponsor ship of the U. S. Air Force Materials Laboratory.

SECTION II

EXPERIMENTAL APPROACH

A. Heating Techniques

As stated the objective of the present study was to explore the melting phenomena of graphite using external heating techniques, and to attempt a resolution of the data with data produced in studies employing resistance heating. The techniques which were used to generate the heating on the external surface of the specimens were twofold namely heating by electric arc and photon radiation from a ruby laser. The source of the arc radiation used was the GE Mk II High Pressure Arc (see Figure 1). Testing in the electric arc was limited to approximately 180 atm pressure because of structural restraints to the test chamber. The source of the laser radiation was a Maser Optics Laser, Model No. 4500 shown in Figure 2. In the burst mode it could normally operate with a 3/4 inch by 13 inch ruby rod and generate as much as 400 joules of energy; however, it was necessary in the present study to use it with a 5/8" x 7" rod which produced approximately 50 joules of energy.

To obtain a comparison of results with externally heated specimens, a number of models were also heated resistively during the course of the study. To minimize the formation of soot and the effect of temperature gradients in the material, the specimen was housed within a guard heater whose heating could be controlled independently of the model. The experimental apparatus which was used for resistance heating is shown in Figure 3.

B. Test Materials

Two graphite materials were investigated in this study. They were chosen to represent differing degrees of purity and were explored to examine the magnitude of any effect of that parameter on the melting process. The higher purity material was pyrolytic graphite (PG) manufactured by chemical-vapor-deposition onto a purified graphite substrate from purified methane or natural gas. The second material examined was ATJ-S, a coke-base graphite manufactured by the Union Carbide Corporation. A comparison of impurities present in these materials is shown in Table I. The pyrolytic graphite data has been obtained by GE and is typical of commercially available material. The ATJ-S measurements represent data obtained on the billet used in the present program. Also shown in Table I for comparison are data for purified ATJ material. It is evident from the data that nominally ATJ-S contains one to two orders of magnitude more alkali and elemental species than pyrolytic graphite.

C. Instrumentation

Surface temperature measurements in this program were made with a scanning spectrometer and an optical pyrometer. A Warner and Swasey Model 501 Scanning Spectrometer was used to monitor material temperatures for the electric arc and laser heating modes. This instrument was operated with detectors and filters which produced optical coverage of the specimen emitted radiation from 1.4 to 3.0 microns (indium arsenide) and 2.5 to 4.4 microns (indium antimonide). From the large body of data that was generated, surface temperatures were determined. In order to handle and process the enormous amount of information obtained, it was necessary to automate the data reduction procedure. Details of this are presented later in this report.

Additional measurements of temperature were made with a Leeds and Northrop Model 8641 Automatic Optical Pyrometer. This instrument has a null balance measuring system employing a fast responding photomultiplier tube as a detector and includes an automatic gain control for optimum operation over a wide range of radiant energy. Instrument response time limited its use to the direct electrical heating technique as the arc heating and laser heating tests were conducted for relatively short times.

SECTION III

SPECIMEN HEATING BY ELECTRIC ARC

One of the sources for external heating of the graphite material was an electric arc and the facility in which these heating environments were generated was the Mk II Arc Heater shown in Figure 1. Unlike most other plasma facilities which generate the heating environment by convection from a high temperature plasma, the Mk II employed direct arc column radiation to raise the specimens to the melting condition. An added measure to this heating method was an incremental amount of ohmic heating which resulted from refinements which evolved during the course of the present study. Initially the program employed arc radiation alone.

A. Arc Radiation Heating

The arrangement used for radiative heating in the Mk II arc facility at the onset of the program is depicted in Figure 4. As with all plasma facilities a continuous gas flow was required for the Mk II for proper operation.

Gas entered the reservoir chamber on the top and expanded through the nozzle into the test section within the perimeter formed by the arc path arbitrarily shown in the figure. Thereafter, it passed over the specimen, and exited from the rear of the chamber. The perimeter of electric arcs which provided the heating are shown schematically in a plane nominally normal to the flow direction at a location between the nozzle and the specimen.

By controlling an electric arc in a high pressure environment a large amount of radiative heat transfer can be generated. This can be shown by referring to Figure 5 where arc radiant intensity is shown as a function of arc temperature for a 100 atmosphere pressure environment. These results which were obtained from Reference 10 apply to the Mk II Arc Heater. Using these data of Reference 10 calculations were made describing the energy available by radiation from a high pressure arc source and in particular for the configuration used in the Mk II arc heater. The results of this analysis show that radiative heating rates of the order of 10 KW/cm^2 are obtainable in such a facility. Values in excess of 9 KW/cm^2 have actually been measured.

Tests were run in the Mk II arc heater set up in the manner shown in Figure 4, whereby the heating was derived solely by radiation from the arc alone. Both nitrogen and argon environments were used. The test mode was subsonic thereby minimizing the velocity of the flow over the specimen to increase the probability of containing the molten material on the specimen

surface during and after test.

Initial operation was with a 1/16" diameter throat to keep the flow to a minimum; however, this did not provide sufficient mass flow to equilibrate arc operation and electrical breakdowns (shorting) occurred. It was further observed that the low flow through the 1/16" throat was not sufficient to keep the optical viewing path to the model fully purged of vaporized electrode matter and clean at all times. To alleviate these conditions larger throats, as great as 1/4" diameter, were incorporated.

This arrangement created other difficulties; it was not possible to keep the arc from being extinguished by the incoming cold gas. To alleviate this an attempt was made to guide the gas by the arc filaments and over the models. A sketch of the arrangement to do this is shown in Figure 6. While this maintained arc operation it did not resolve all of the viewing port difficulties. The electrode matter was kept out of the optical path, however, arc radiation was not.

Continued testing pursuing mechanical exclusion of arc illumination did not succeed and further there was no evidence of surface melting of the test specimens. To increase specimen heating required the location of the specimen closer to the arc source. To do this, keep the arc from extinguishing and minimize arc illumination a different electrode arrangement was employed. This is shown graphically in Figure 7.

Unlike the previous electrode geometry which produced a number of arcs in a plane, the modified arrangement resorted to a single arc filament stretching between a central rod and a concentric, annularly tapered surface. With this geometry, gas entered tangentially into the upper electrode chamber passing around the rod (anode) and through the annular cathode. This mode of entry for the gas enhanced arc rotation within the annular space between the two electrodes, stretching and thereby constricting the arc filament. The rapid rotation also resulted in uniform surface heating. In addition to this gas flow a smaller fraction of gas (10-20%) was admitted through the anode electrode to purge the optical path to the model of any carbon vapor thereby assisting the measurement of surface temperature.

Using this electrode geometry it was possible to double the electrical power being dissipated and also to position the arc filament closer to the specimen surface. The models which were also modified to minimize specimen heat transfer loss through conduction to the holder also helped to attain higher temperature conditions. This latter modification was affected by reducing the holder wall thickness to 1/32" and reducing specimen thickness to an 1/8". This was about one-half the original dimensions for both holder and specimen. A typical model is also shown in Figure 7.

This method of performing the experiments clearly was an improvement over the previous technique. Examination of specimens after test showed evidence of resolidification on the surface. A typical specimen is shown in Figure 8. Furthermore the continued movement of the arc filament over the electrodes and the larger size of the electrodes minimized electrode degradation. This made it possible to run for longer times and allowed for the use of the optical pyrometer in addition to the spectrometer for measuring surface temperature.

Although specimen heating was improved and melting occurred using this approach the existence of undesirable arc reflections continued. The various approaches that had been explored previously had included: a) the use of a small orifice (throat) between the plane of the electrodes and the viewing port; b) increasing the orifice thereby increasing the mass flow of gas to isolate the arc nearer to the wall of the arc chamber; c) the use of cylindrical extensions to the optical port moving the inlet of the port closer to the specimen surface; and d) an attempt to contain the arc in an annular region away from the viewing port opening. All these were unsuccessful in eliminating arc reflections; it was therefore concluded that the heated surface observed by the optical sensors had to be totally isolated from the arc. To do this yet locate the arc at the specimen for heating purposes required another change in the testing technique. An arrangement was developed which not only produced heating due to arc radiation but also contributed ohmic heating as well.

B. Arc Radiation and Ohmic Heating

The test configuration that was finally employed is shown in Figure 9. Basically, the end of the anode was sealed off with only four bleed holes provided to allow flow over the backside of the closed off electrode. By making the face of the anode the test material it was exposed both to ohmic heating and arc radiation. At no time during the nominal test time therefore was the arc radiation detectable by the optical temperature sensors.

A test was conducted by focusing the sensors on the back face through the regular optical window. After the arc heater was activated, the front surface of the specimen was heated instantly and shortly thereafter the rear surface temperature began to increase. The front surface quickly came to the melt temperature (assuming the pressure level was adequate) and began to recede. As this occurred the rear surface also began to increase its temperature very rapidly. The closer the two surfaces approached one another, the closer the rear surface temperature approached that of the melting front surface. When the two surfaces were approximately .010" apart the temperature difference was of the order of 50°K (see Figure 10). As the front surface broke through to the rear surface the temperature sensor signal decreased rapidly due to the removal of radiation surface area and the cooling effect of

flow through the eroded specimen. This decrease in signal continued as the orifice in the specimen grew larger. Eventually it became negligible and only increased again when the arc filament migrated into view. On some occasions the arc extinguished itself from the increased flow through the specimen. When these events occurred a test was terminated; typical sensor signals recorded from a test are shown in Figure 11.

As mentioned, a test was terminated when the front surface eroded completely to the back of the specimen. Since the heating time was adjusted a priori to terminate a test when only part of the rear surface had been eroded away, the resulting specimen at the end of a test had a hole in it (see Figure 12). The material remaining on the front surface was characteristically similar to that which occupied the opening prior to its being eroded. By observing the physical characteristics and the microstructure of such a specimen, it was possible to ascertain whether melting had occurred. Specimens that had experienced melting always had resolidified material remaining on the front surface. This was similar in appearance to the photograph shown in Figure 8 for pyrolytic graphite and Figure 18 for ATJ-S material. Whereas the pyrolytic material formed definite droplets, the ATJ-S resolidification was in the form primarily of smooth rivulets however there were also some droplets. In contrast to this any vapor deposition that occurred during a test showed up as a fine powder on the surface. The latter had very low adherence to the surface as compared to the droplet or rivulet formations.

Earlier it was stated that the temperature gradient across the specimen approached insignificant values as the front surface receded into close proximity of the rear surface. This can be seen graphically in Figure 10. The calculations plotted there are for ATJ material heated at the rate of 10 KW/cm^2 typical of the arc environment. The curves shown represent the temperature distribution through the material as the front surface heats to a nominal temperature of 4000°K representative of the melting value and is maintained at that level. Although the calculation did not take into account surface recession, the effect of the front surface moving towards the rear can be qualitatively established by observing the temperature distributions as X/L decreases to zero. It can be seen that the temperature difference for the 1.0 and 1.5 seconds of elapsed time (typical test times) is indeed very small for $X/L \approx 0$ so that when the rear surface temperature is recorded, front surface temperature can be determined from those values.

SECTION IV

RESISTIVE HEATING OF SPECIMENS

To study the melting phenomena by resistively heating the graphite material it was necessary to design and fabricate a special test apparatus. The resulting test chamber is shown in Figures 3a and 3b. The design of the unit provided for separately heated specimens and an annular guard heater to minimize heat transfer losses from the specimen. This flexibility was accomplished by designing two controllable ballast resistors (Figure 13) and placing one in series with the specimen and the other with the guard heater and then connecting the specimen and guard heater circuits in parallel with each other. The electrical circuits were sized such that over 3500 amps could be drawn from the battery power supply, and provision was made in the chamber design for handling the high heat loads and the thermal expansion of the various parts. Access for surface temperature measurements was provided through an optical port located in the bottom of the chamber while the optical path was kept clear by a purging arrangement. This was done by injecting the test gas through the sight tube (see Figure 3b). The gas then passed into the specimen compartment, over the specimen and exited from the chamber. Entry of the gas at the bottom with the guard heater arrangement was chosen to enhance the normal free convection flow of any vapor within the test unit thereby moving such vapor through the chamber as rapidly as possible before condensation occurred.

The test procedure was initiated by pressurizing the chamber to the desired value and maintaining a constant flow of gas through the optical port using a controlled leak. Orifices as small as 0.003" diameter were used for this purpose and were located at the exit of the upper exhaust holes shown in the drawing of the test chamber in Figure 3b. After pressurization, electric power was applied in various combinations to both the guard and specimen circuits and varying heating times were used. Current values were increased until specimen failure occurred. Usually this was due to the onset of melting but in one or two instances electrical breakdown occurred without melting. It was hypothesized that the failure without melting was the result of fracture at a flaw in the material or one triggered by a microscopic fracture that had occurred during specimen fabrication. When the electrical power was shut off the pressure in the chamber was maintained until the specimen had cooled down to low values of temperature. Throughout the test the internal surface of the specimen was observed by an optical sensor and the temperature history was recorded. Heating cycles varied from approximately 30 seconds to 3 minutes. Details of these are described later.

ATJ-S and pyrolytic graphite materials were both tested using generally the same specimen configuration. A number of arrangements were explored and these are shown in Figure 14. Initially the specimens were 1/2 inch cylinders with a cavity indentation as shown in Figure 14a. As current was applied to those specimens their temperature increased until for the appropriate pressure levels melting occurred. At these high temperature conditions thermal expansion occurred resulting in an increase in specimen cross section; in some cases specimens actually burst open as shown in the sectioned model in Figure 15. This behavior was minimized by venting the central portion of the specimen with a 1/8" hole along the axis and radial holes intersecting this at each end of the specimen (Figure 14b). This arrangement provided relief for the melt material and tended to decrease pressure gradients across the material cross section. However, as the specimens advanced to the melt condition the vent holes and the viewing cavity filled with a combination of melt and deposited vapor. It was not clear whether these deposits were affecting observation of the specimen surface therefore, additional steps were taken to eliminate this occurrence along with attempts to increase the heating in the vicinity of the test cavity.

To get added heating the arrangement shown in Figure 14c which made use of a smaller specimen was used, while the modification presented in Figure 14d was adopted to minimize or eliminate vapor deposition. Notice that an extra vent hole was added perpendicular to both the longitudinal vent hole and the viewing cavity for increased gas flow. Besides these specimen changes the optical sight tube was extended through the guard heater to within 1/16" of the cavity opening where the clean purge gas could more easily blow away any vapor generated around the cavity. This arrangement, Figure 14d, was the final configuration and the one used to generate the test data.

As indicated previously, optical observation of the heated specimens was made at the internal surface and due to the various cutouts in the center of the test pieces, that location showed the earliest occurrence of the melting condition. A typical specimen after test is shown in Figure 16.

SECTION V

SPECIMEN HEATING BY LASER

The pulsed laser used for these tests (see Figure 2) operated at the ruby wavelength of 6943 Å. It is comprised of a cylindrical ruby crystal which serves as the active medium, pumped by two 12 inch Xenon flash lamps mounted in a doubly elliptical silvered flash cavity. The ruby crystal which is usually used for burst mode operation is a 3/4 x 13 inch rod having one flat front face and a chisel TIR cut on the rear. A second smaller crystal rod 5/8" x 7" having flat plane parallel ends is generally used for the Q-switched mode.

A. Laser Facility Preparation

Because the laser was located in another part of the plant it was necessary during this study to move the laser facility to the site of the high pressure test chambers. In addition to comply with current laser safety requirements a separate room had to be constructed to house the laser in the arc laboratory. Due to the large physical size of the laser and other space limitations the output of the laser could not be brought closer than 30 feet from the high pressure chamber.

Tests made on the large Vernuli grown ruby crystal (13" rod) indicated that the quality of the material, and accuracy of the TIR chisel cut were not high enough to operate effectively over such a distance. The smaller 5/8 x 7 inch ruby rod was therefore modified so as to operate in the burst mode. This was accomplished by replacing the Pockel cell with a concave 10 meter focal length dielectric reflector. In order to accurately align the resonant cavity two precision optical alignment devices were installed. Adaptors were then designed and fabricated which allowed the optical positioners to accept either Q-switched or burst mode optics with minimum realignment. The front adaptor was also designed to hold any number of sapphire etalons without imposing any distortion in the system.

An experiment was performed to determine the laser threshold energy. It was found that using ten 375 microfarad (μf) capacitors with no series choke, a minimum energy of 12, 675 joules was needed to obtain lasing. This was determined by measuring the level at which incipient vaporization could be observed on blackened Polaroid film. This threshold energy was also measured as a function of the output reflectance of the resonance cavity. Best results were achieved with two Czochralski etalons. The beam divergence of the laser was reduced by maintaining a large distance between the resonant reflectors (approximately 5 feet) and limiting the exit aperture to a 3/4 inch diameter opening.

B. Laser Pulse Broadening

In order to enhance the recording of good temperature data a long (~ 10 millisecond) duration burst of laser light was desired. Since this is approximately an order of magnitude longer than standard burst mode lasers, an attempt was made to modify the laser accordingly. The method of approach chosen called for the optical pumping of the laser to be modified so as to provide an intensity slightly greater than threshold for a period of 10 milliseconds.

In order to meet this requirement a number of changes had to be made in the flashlamp energizing circuitry. The RC time constant of the circuit was increased by connecting the flash amps in series as opposed to the original independent parallel configuration. Since in the former design each lamp was pumped by a separate capacitor bank and triggering circuit, this entailed a modification of the pumping electronics. The flashlamps were rewired at the laser head and the current routed so as to conform with the polarity requirements of the lamps. The capacitor banks were rewired so as to have six banks containing five $375 \mu\text{f}$, 4 KV capacitors tied in series instead of the original two banks. The emergency discharge, charging, control and interlock circuitry also required modifications.

One of the major difficulties encountered in the modified mode of operation was that a single trigger transformer was required to fire both flashlamps. It was found that due to the higher impedance of this series configuration, even with the trigger level set at maximum the lamps failed to ionize. The two original trigger transformers could not be wired in series due to the inherent jitter in the system which prevented simultaneous firing. In order to provide the maximum signal and minimize transmission losses, the trigger generator was moved as close as possible to the flashlamps. Although this relocation provided some improvement, the lamps still failed to trigger reliably. The problem was finally eliminated, however, by insulating the reflecting cavity from ground and connecting it to the positive terminal of the flashlamp. The resulting fields produced by the proximity of the charged cavity assured reliable triggering of the lamps.

Once repeatable triggering of the laser had been obtained a measurement was performed to determine the minimum capacitor charging voltage which would supply sufficient current to maintain flashlamp ionization. This voltage was found to be approximately 500 volts and allowing for a safety factor of two, the capacitor voltage was maintained just above 1,000 volts. Laser performance was then determined. This involved establishing both the current-voltage characteristics of the flashlamps and making calorimetric measurements of the laser photon output.

C. Specimen Tests

Following laser calibration, experiments were conducted to impact a material specimen in a pressurized chamber with laser energy. Due to the design of the pressure vessel the graphite test specimen could not be positioned closer than 7 inches behind the 3/4" diameter entrance window. For this reason a relatively long focal length lens was used in order both to reduce the beam diameter sufficiently to pass through the entrance window and also to focus the beam by using a pair of high quality lenses having minimum spherical aberration at 6043 Å and four to one focal length ratio. After a few shots, however, these lenses showed signs of severe degradation due to pitting near the central axis. This was probably caused by light reflected from the curved surface of one lens being focused onto the other. In order to avoid further damage to the pair, a single condensing lens was substituted in the remaining experiments.

Alignment of the laser optical system with the specimen was performed by means of an auxiliary helium-neon laser. Initial tests were conducted with ATJ-S graphite. Pressure levels were in excess of 100 atmospheres and argon was the test gas. A number of tests were conducted using this arrangement, however, optical difficulties persisted and no melted specimens were generated. Additional details are presented in the later discussion.

SECTION VI

SURFACE TEMPERATURE MEASUREMENT

Specimen surface temperature measurements were made using two different instrumentation techniques. This involved the use of the Warner and Swasey Model 501 Scanning Spectrometer and the Leeds and Northrup Model 8641 Automatic Optical Pyrometer. Although the application of the former was more complex and required considerably more effort to reduce the data, it had the necessary rapid response to obtain data in the arc and laser environments. To handle the voluminous amount of data generated by the spectrometer much of the data reduction procedure had to be automated. The optical pyrometer was initially used in both the arc and resistance heating tests, however, as the study progressed arc test times decreased in length whereby the pyrometer could no longer be used in those environments. The result was that pyrometer data were obtained only with resistance heated specimens.

A. Description of Scanning Spectrometer

The Warner and Swasey Model 501 Scanning Spectrometer consists of four major components which function together to provide data. They are an energy collecting optical system, a Czerny-Turner type spectrometer, the rotating scanner-drum and photo-detectors.

Radiation is collected by a Cassegrainian telescope; the secondary mirror remains fixed while the primary can be adjusted for focusing. The effect of this arrangement is to keep the image formed by the telescope always in focus at the entrance slit of the spectrometer.

The spectrometer, because of the basic arrangement of its components is called a Czerny-Turner. Dispersion is obtained with a grating ruled to disperse the energy to a degree compatible with the detectors. The Warner and Swasey instrument has a series of fixed-width slits at both exit and entrance of the spectrometer - an innovation employed to identify slit widths with absolute certainty. A scanning drum located at the midpoint of the optical path in the spectrometer is belt driven by one of several motors. Maximum driving speed provides approximately one scan per millisecond. On the periphery of the drum are mounted 24 equally spaced pairs of mirrors with each mirror of a pair facing the other at an inclination of 45 degrees with respect to a common radius of the drum. The displacement of each pair as the drum rotates produces the displacement of light necessary to produce one scan. The dispersed energies are split and directed along two separate paths to the detectors.

The instrument can be installed with various detectors and is presently operating with detectors which are indium arsenide (1.4μ to 3.0μ) and indium antimonide (2.5μ to 4.4μ). The two portions of the spectrum covered by the detectors share a small region in the vicinity of 3μ . Both detectors are refrigerated with liquid nitrogen to increase their sensitivity.

The scanning spectrometer has several additional features, the most important of these being a reference globar which functions as a self-contained reference source. The globar has characteristic radiation that is quite gray in the portion of the spectrum being employed.

B. Spectrometer Optics

Absolute measurements of spectral radiance were predicated on filling the spectrometer's Cassegranian mirror optical system. As long as this condition was fulfilled the instrument could be used to make direct comparisons between an unknown source and a blackbody standard source. A characteristic of the optical system is that it has a constant f number, so the comparison did not have to be made at the same source distances, but any differences in absorption along the optical path had to be considered.

Two conflicting requirements had to be met to fill the spectrometer optics. First, the effective source image had to be sufficiently large to fill the spectrometer entrance slit and secondly the source radiation solid angle had to be such that the entire source was visible over the entire spectrometer primary collecting mirror surface. To satisfy these bounds a stop plate was made reducing the normal spectrometer optical opening from an effective diameter of 4.5 inches to one of 3.5 inches. While this resulted in a 50% decrease to the effective Cassegranian collecting area it established the proper control of the radiation source. It produced an arrangement whereby thermal gradients across the effective source were negligible and instrument alignment was not sensitive.

C. Temperature from Spectrometer Data

Data obtained from the Warner and Swasey spectrometer were in the form of repeated scans of infrared emission in the 1.4 - 3.0μ and 2.5 - 4.4μ regions. The objective in data reduction was to convert this information to temperature, utilizing the Planck radiation equation. For this purpose the output of the detectors was FM recorded on magnetic tape. The raw data tape was then run through an analog-digital (A-D) conversion to produce a new, digitized, tape and small scale analog plots from which specific scans were selected for further processing. The selected digitized scans were then processed by program SPECT to deduce absolute temperature.

D. Analysis of Spectrometer Signal Interpretation

A body with spectral radiance N_λ (watt/cm²-str- μ) produces a processed response S_λ of an integral number of digital "counts". The relation between N_λ and S_λ can be expressed as,

$$S_\lambda = N_\lambda \tau_\lambda R_\lambda G \quad (1)$$

where τ_λ is the transmissivity of the optical path, R_λ is the response of the radiation detector and G is system gain. The factor G is independent of wavelength and is the product of all the gains or attenuations associated with preamplifiers, recorder and A-D converter. The response factor can be eliminated by taking the ratio of the signal from an unknown source (subscript u) to that from a known temperature black body (subscript b). This can be written

$$\frac{S_{\lambda,u}}{S_{\lambda,b}} = \left(\frac{N_{\lambda,u}}{N_{\lambda,b}} \right) \left(\frac{\tau_{\lambda,u}}{\tau_{\lambda,b}} \right) \left(\frac{G_u}{G_b} \right) \quad (2)$$

Further the spectrometer has mounted within it a tungsten carbide "glo-bar", maintained at fixed spectral radiance, which can also be observed by the detectors. Therefore, the relative response of an unknown source to a known source (black body) at a fixed wavelength (λ_g), optical path, and global radiance, can be written in terms of the ratio of the response of each to the global as

$$\frac{S_{g,u}}{S_{g,b}} = \frac{G_u}{G_b} \quad (3)$$

Thus, global reference scans supply a permanent record of comparative system gain, except for step changes made when switching from global to external source. Since the black body used for calibration was maintained at 1000°C, its radiance was significantly weaker than that from the unknown and additional gain was necessary with the black body signal to obtain comparable digital resolution.

Now the Planck equation relates spectral radiance to temperature as,

$$N_{\lambda} = \frac{C_1 \epsilon}{\lambda^5 (e^{C_2/\lambda T} - 1)} \quad (4)$$

where C_1 and C_2 are constants and ϵ is emissivity ($\epsilon_b = 1$, ϵ_u is, in general, a function of both λ and T).

If

$$\alpha_{\lambda} = \frac{C_1 \epsilon}{N_{\lambda} \lambda^5} \quad (5)$$

Then

$$\frac{\alpha_{\lambda,u}}{\alpha_{\lambda,b}} = \epsilon_u \frac{N_{\lambda,b}}{N_{\lambda,u}} \quad (6)$$

Combining Eqs. (2), (3), (5), (6)

$$\alpha_{\lambda,u} = \epsilon_u \left(e^{C_2/\lambda T_b} - 1 \right) \left(\frac{S_{\lambda,b}/S_{g,b}}{S_{\lambda,u}/S_{g,u}} \right) \left(\frac{\tau_{\lambda,u}}{\tau_{\lambda,b}} \right) \quad (7)$$

Transmissivity ratio can either be determined by separate spectrometer measurements or made unity by observing black body and unknown sources via equivalent optical paths. Thus emissivity is the only factor in the expression which is not known or susceptible to direct measurement. For simplicity in the data reduction emissivity (ϵ) was chosen to be unity.

Setting $\epsilon = 1$ leads to a "brightness temperature" which establishes a lower bound on the true temperature of the radiating source. Referring to Eq. (4) this then becomes

$$T_u = \frac{C_2}{\lambda \ln(1 + \alpha_{\lambda, u})} \quad (8)$$

Wavelengths actually used for temperature computation were restricted to those locations on the wavelength scan from which the observed intensity was insensitive to small changes in wavelength, thus minimizing the effect of small errors in wavelength calibration. The actual wavelengths used for computing temperature values were 2.10, 2.15, 2.20, 2.25, 2.30, 2.35, 2.40, and 2.45 microns from the short wavelength scans and 3.05, 3.10, 3.15, 3.20, 3.25, 3.30, 3.35, 3.40, 3.45, 3.50, 3.55, 3.60, 3.65, 3.70, 3.75, 3.80, 3.85, 3.90, 3.95, 4.00, and 4.05 microns from the long wavelength scans.

A procedure was also worked out⁽¹¹⁾ for computing temperature based on the slope of the intensity vs. wavelength curve assuming the source was a gray body. This method could have eliminated the necessity for absolute intensity calibration or permitted computation of emissivity. Unfortunately, the infrared bands which were observed were quite far from the peak of the black body curve so that a very small error in slope resulted in a very large error in temperature. Thus these results were unreliable and primary emphasis was placed on absolute intensity measurements as discussed above.

E. Spectrometer Wavelength Calibration

The waveform of the output of each detector as shown in Figure 17 reflects the combined effects of detector responsivity, system frequency response, cut-off filters and atmospheric absorption. For any continuous radiation source the shape changes relatively little with temperature and this fact was utilized in establishing wavelength calibrations. Two types were desired:

- a) an initial calibration to establish reference points on the spectra as precisely as possible
- b) routine calibration using these reference points performed for those scans from which temperature was determined

The initial calibration made use of both filter absorption lines and arc lamp emission lines of well known wavelength. The emission lines were assumed

to have a natural profile and the absorption lines a Gaussian profile. The curves assumed for the reference points were empirically chosen to fit the observed spectra.

All observed spectra, including those used for initial calibration were converted to digital form. Therefore location of a specific feature (e. g. a line peak) which might, in general, fall between sampled points, was accomplished by least squares fit of an appropriate curve except for the initial ramps. The curves were all expressed in the form:

$$y_n = \frac{y-A}{B} = f(C, x-D) \quad (9)$$

Constants A and B were determined by defining a function (see Reference 12)

$$F = \sum_i \left\{ A + [B f(C, x_i - D)] - y_i \right\}^2 \quad (10)$$

and setting

$$\frac{\partial F}{\partial A} = 0 ; \quad \frac{\partial F}{\partial B} = 0 \quad (11)$$

The parameter C is a characteristic of the particular feature being fitted and was established directly from the analog plots or from several sets of digital data. The quantity D is the wavelength (expressed in units of digital word spacing) of the feature of interest. Since $f(C, x-D)$ was generally non-linear, an automatic iteration procedure was used to find that value of D for which the data best fit the assumed functions. In the case of the initial ramps the intersection of a zero level line and a straight line fitted to the first few points on the ramp proved most reliable. Zero level was obtained on the basis of a digital filtering procedure developed by Martin (Reference 11) and the ramp was determined by a least squares fit.

SECTION VII

RESULTS AND DISCUSSION

A. Arc Heating

As previously indicated a significant effort during the study was directed toward the generation of material specimens which had experienced melting. After trying a number of approaches the technique that was employed to provide test data was that of using both arc radiation and ohmic heating to raise the material to melting conditions and obtaining the temperature of this occurrence by monitoring the specimen back face temperature during the heating cycle. In this manner the temperature measurement could be made without the concern that extraneous radiation from the arc itself would affect the optical radiation measurement.

Data were obtained with both ATJ-S and pyrolytic graphite specimens (ab-plane heated) and testing was performed using both argon and nitrogen gas. The range of pressure explored in this phase of the work varied from 95 atm to 180 atm, the upper limitation being established by the structural limitations of the arc facility. Although arc testing was conducted over this range of pressure it was only possible to generate sufficient heating to bring on the onset of melt at pressures in excess of 135 atm. Since radiative heating is a strong function of plasma density level, it would appear that the radiance dropped off rapidly below 135 atm. This is not at all conflicting with previous statements made in this report about the radiance attainable in high pressure arcs. The information discussed previously referred to constricted arcs whereas in the testing mode employed in this study, constriction, mechanical or fluidized was small. Nonetheless a considerable amount of data was obtained on melting at the elevated pressures.

Typical specimens tested in the arc environments with nitrogen are shown after test in Figures 18 and 19. The ATJ-S specimens in Figure 18 represent specimen appearance before and after burn-through. Note in that figure that the heating was applied uniformly axi-symmetrically and that the burn-through started in the center of the specimen. Surface resolidification is visible in both specimens and shows up as solidified rivulets and occasional spheres over the entire surface. The solidified material should be specimen material and not holder material since during test the front surface of the specimen was facing downwards. The resulting primary resolidification pattern, namely the rivulets, may have been influenced by specimen orientation in the facility.

The pyrolytic graphite specimen in Figure 19 also shows the front surface having receded to the back face. The photograph is looking normal to the ab planes. The dark spot in the center is a piece of photographic paper used to outline the hole in the specimen. Surface texture is clearly different than that shown in Figure 18 for ATJ-S. Not only is there a lack of a rivulet formation by the solidified liquid but the amount of solidified matter on the surface is much less. The small dark spots that are visible on the un-eroded material are solidified matter generally in spherical shape. This difference between the two materials indicates perhaps that the liquid may not wet the pyrolytic graphite as well as it does ATJ-S. There is no reason to suspect any significant difference in liquid viscosity; more likely it may be due to differences in surface roughness affecting the flow and adhesion of the melt. Another point of interest is the apparent high reflectivity of the pyrolytic graphite when compared to the ATJ-S material. Whereas only the solidified melt is highly reflective on the ATJ-S specimen, the entire surface of the pyrolytic graphite has that appearance. Although no pretest specimen is shown for comparison, the end of test reflectivity was considerably greater. General appearance of both materials appeared to be the same regardless of whether the tests were conducted in argon or nitrogen. Details of the material microstructure are discussed later in the report.

Temperature observations of all specimens were made with the scanning spectrometer. Since the effective area on which the instrument was focused was approximately 5% of the diameter of the front surface of the specimen, the gradient in temperature across the observed area should have been negligible. This should be the case as long as the front surface breaks through to the rear surface of the specimen more or less on center. This was the case in all the tests that were performed. Slight departures from the exact center should not have any significant effect. Examination of the sampling time of the spectrometer instrument also indicates negligible effects. Recession rate of the test specimens was such that in one scan of the instrument not more than 1-1/2 mils of the material would be eroded. Based upon the conduction calculations discussed earlier this would work out to be about 5°K change in temperature during a scan at the melting conditions (~ 4000°K).

B. Resistance Heating

ATJ-S and pyrolytic graphite specimens were heated resistively over a range of pressure from 95 atm to 310 atm in both argon and nitrogen environments. A typical specimen is shown in Figure 16 at the conclusion of a test. The fracture at the location of the viewing port occurred during test and generally was the means by which an experiment was terminated.

During the heating cycle there was no evidence of vapor obstructing the optical path. The optical window, the steel sight tube and the graphite

extension were completely free of any vapor (soot) deposits. There was also no indication of vapor deposition in the cavity at various time periods into a run. This was determined by aborting tests to examine for vapor deposits. It was difficult however to detect the precise onset of vapor deposition in the specimen cavity. The first indication of any change in conditions was the erratic behavior of the temperature and electrical power sensors. This erratic performance lasted for approximately one to five seconds. Immediate test termination after the start of such behavior always showed some evidence of vapor deposition and resolidification in the test specimen. The longer a test continued once the erratic behavior began, the more vapor deposition and resolidification was present on the specimen upon cool down. At no time did a specimen show melt at the end of a test without the sensor fluctuations occurring.

Even though there was considerable resolidified material on a specimen at the termination of a test it was not possible to identify when the optical sensor was observing such material. Melting was initiated within the thickness of the specimen and progressed toward the outer diameter, however, since electrical conditions were also changing as this occurred, the time when melt showed up at the specimen surface could not be pinpointed. While the light fluctuations which occurred might be construed to be representative of differences in the reflectance of solid and liquid material, since the optical sensor could not resolve anything smaller than a 0.10 inch diameter (target area), precise identification of melt alone was not possible. Another factor to confuse the issue is the possible occurrence of arcing across local failures in the specimen. The intense radiance of high pressure arcs was described earlier; this radiance could definitely affect or even override any differentiation in the radiation from a solid or liquid surface. Incident light reflections were visible off the face of the temperature sensor, and this could be interpreted as a confirmation of the occurrence of arcing. In the final analysis however since all the events described happened in such rapid succession it was virtually impossible to affect a complete resolution.

Specimens such as those shown in Figure 16 generally showed evidence of large amounts of melt resolidified over the entire crosssection in the region of the cavity. The material was usually in the form of highly reflective globules. In most cases a solidified concentration was present in the graphite above the optical cavity and generally a large more or less spherical globule could be found clinging to the upper portion of the cavity. On many tests the melted material appeared to have flowed into the various drilled holes in the specimen at the region of the cavity. Some of this material was collected and examined microstructurally. A discussion of such analyses is presented later in this report.

Some difficulty was encountered in the testing of pyrolytic graphite specimens in the resistance heater. Because of its anisotropic thermal

characteristics it was difficult to heat the material without delamination occurring. While heating cycles for both materials were very similar, when fracture occurred and a test was terminated the pyrolytic graphite specimens showed very little resistance to delamination. This was true regardless whether the cavity was oriented normal to or in line with the ab planes of the material.

The optical cavity shown in the specimen in Figure 16 shows evidence of vapor deposition. It was indicated previously that the optical sight tube was the inlet tube for gas flowing into the test chamber. Although the flow was minimal it was positive. Nevertheless while the sides of the cavity region showed no evidence of vapor deposition there was evidence of vapor deposited in the lengthwise center hole through the specimen in the vicinity of the cavity.

Various heating cycles were employed to control the presence of deposited vapor. Both the guard heater and the specimen power were varied independently. Low power levels were applied to both circuits initially (300-500 amps) and then depending upon the test objective the power was either increased slowly or rapidly until melt occurred in the specimen. While the specimen was being heated varying conditions were imposed upon the guard heater. Situations were examined in which the guard heater was held either close to specimen temperature or at lower levels of temperature, as low as the initial power-on values. This produced a guard heater temperature range from 1000°K to 3300°K. Regardless of this, examination of the specimens after test did not show any noticeable difference in vapor deposition. The only apparent difference was that it required less power to heat the specimen to melt when the guard heater was held at the higher temperatures. One explanation for the minimal effect of the guard heater might be the fact that the optical port was extended to the immediate vicinity of the test specimen cavity in all the testing. In essence the finite velocity of the purge gas as it entered the specimen cavity may have been the controlling factor in minimizing vapor condensation at that location.

A plausible explanation of the vapor deposits seen on the specimens after test is that they did not occur until the tests were terminated. This might be inferred from examining Figure 16 where the vapor is shown on the resolidified globule. This suggests that the molten material had to cool below the vaporization temperature before vapor could condense upon it. This is highly probable since in all resistance tests the pressure was maintained well after the specimen cooled down. Once the specimen fractured it lost power and cooled rapidly. The guard heater circuit was still intact so that vapor could have been generated before the operator disconnected the power. In this manner the vapor could condense on the cooled specimen and would support the theory that the vapor deposit did not hinder the observance of that surface on which the optical sensor was focused during heating.

Examination of the specimens heated rapidly (as low as 30 sec) and slowly (as long as 3 min) did not reveal any detectable difference in melt temperature within the scatter of the data. The only effect of the rapid heating was an indication of a lesser amount of vapor deposit on some models. However, since it did not appear to affect the measured temperature values this slight difference in vapor deposition was not a factor in evaluating material performance.

C. Laser Heating

The use of laser heating in this study did not produce the onset of melting. During a number of the laser firings the entrance window to the pressure chamber was found to be "burned" on the high pressure side. This deterioration of the optics indicates that the pressurized gas was being ionized to an unusually high degree. This type of breakdown frequently has been observed in the case of high power Q-switched lasers but is quite unusual in relatively low power burst mode lasers such as the one used in this study. The ionization was most clearly evident when an auxiliary lens was positioned just behind the entrance window inside the pressure vessel. After the laser was fired both the window and lens were severely degraded on their adjacent surfaces. This seems to imply that dielectric breakdown of the argon (test gas) was induced by the high electric field of the laser beam and that the resulting plasma was inhibited from expanding by the presence of the lens. The increased ion concentration caused by this constraint in turn increased the absorptivity of the plasma. It can thus be seen that this type of plasma formation within the pressure chamber can significantly reduce the amount of laser energy which reaches the test specimen. This rather unexpected high pressure phenomenon has not been reported to date in the literature and should be investigated more thoroughly before other quantitative laser studies in high pressure environments are attempted.

Microscopic examinations of test specimens impacted with the laser show that vaporization occurred. This was evidenced by a slight surface depression in the area of irradiation and the appearance of an annular ring of graphite dust surrounding the depression. The appearance of the dust on the surface can be explained from earlier photographic studies⁽¹³⁾ in which high speed pictures were taken of the blow-off plume. In this study it was observed that whereas the vapor would move off the surface at high velocity in a vacuum, when the pressure was increased to one atmosphere, the plasma remained just above the surface for relatively long periods of time. It would seem extremely likely that at the high pressures utilized in this study that a portion of the vapor would recondense on the cool surface surrounding the depression.

In retrospect it seems that a burst mode laser such as was used in this study was not a suitable heating source. Furthermore it generated a

plume flow at the point of impact which would make temperature measurements difficult to obtain even though none were attempted due to optical problems. A better approach for future studies would be to use a large (~ 10 KW) continuous wave laser which could be adjusted so as to achieve the desired surface temperatures. This would also eliminate the deleterious high pressure ionization effects observed in this study. Such lasers have been developed since this study was undertaken, but none was available for the present work.

D. Microstructure of Solidified Graphite

Selected samples of arc-heated, resistance-heated and laser-heated specimens were sectioned, mounted in acrylic resin, and micro-polished to permit examination of the structures resulting from the solidified liquid. Selected views are presented in Figures 20 to 27, which show the types of crystal morphology. No evidence of liquid was found with the laser-heated specimens, although thinning as a result of vaporization was evident.

Previous studies by Basset⁽¹⁾, Noda⁽⁴⁾ and Schoessow⁽⁶⁾ used the presence of highly perfect crystals or formation of globules as indications of melting. In high-pressure studies, Bundy⁽¹⁴⁾ showed that relatively large, densely-packed crystals grow with ab orientation perpendicular to the solid-liquid interface in superheated samples; these were epitaxial to the unmelted particles when samples were heated with lower power inputs.

The observations in this study are consistent with the prior work and, in addition, provide evidence for large volume contraction during solidification. The morphology is identical to that observed on previous samples which were heated by resistance or by an arc at high pressure under conditions which were less well characterized⁽¹⁵⁾.

Figure 20 illustrates a typical large drop solidified from a resistance heated specimen; note the shape suggesting buckling of the surface due to volume contraction during solidification. As illustrated more clearly under polarized light, Figure 21, the proportion of volume filled by crystals in the material at room temperature is quite small, with some concentration of crystals close to the surface. Quantitative metallography could be used to estimate the density of the liquid based on the filling in of these samples, however, since a part of the material was no doubt lost by vaporization on cool down, there would be some error in the analysis.

Figures 22 to 27 show structures typical of solidification on a surface. Densely packed columnar crystals grew into the melt, and the remaining liquid solidified as platelets with random orientation which impinged during growth to form a low density boxwork. At the wall a fine-grained structure suggests solidification of a liquid-solid mixture, and similar structure was often found

in other portions of the droplets. A very fine crystalline material characteristic of nucleation and condensation from vapor could be clearly distinguished from the material characteristic of solidification. Observations of the unpolished surfaces of the plates showed growth steps and a smooth surface, which led to the shiny appearance of the droplets when first examined after the experiments.

Solidified liquid on the surface of the graphite samples could be clearly distinguished by these characteristic forms, even when only a very thin layer (not immediately apparent at low magnifications) coated the substrate. The presence of liquid in samples of this type is relatively easy to identify.

To pursue the microstructure analysis further, an examination was made of a specimen with a scanning electron microscope. A solidified droplet was chosen for this purpose. Fig. 28 shows growth or evaporation steps at high magnification (2000X) on the basal planes of the graphite crystals both at the surface and in the interior. It also shows that the crystals in this specimen were very thin in some locations. Figures 29 and 30 show the appearance of the droplet before and after sectioning with a razor blade (deformation tended to cover some of the voids on the sectioned surface). Note that on the original solidified surface (Figure 29) the crystals were stacked parallel to the surface and tightly packed. On the other hand in the interior (Figure 30) the crystals were thin flakes and widely separated. This crystal arrangement would tend to support the speculation that while there would have been some evaporative mass loss from the interior of the droplet during cooling after solidification, it was probably held to a minimum.

E. Phase Diagram

The experimental measurements of the temperatures at which melting occurred along with the pressure levels of the occurrence were used to determine the solid-liquid interface of the phase diagram. A plot of brightness temperature results is shown in Figure 31 obtained from arc heated and resistively heated specimen data. Because of hardware pressure limitations the arc data covers only the lower portion of the pressure regime. The occurrence of melting was determined from physical observations of the surface of both the arc heated specimens and the fractured cross sections of the resistively heated specimens, corroborated by microstructural examination. Temperatures at the onset of melting were determined as discussed earlier.

The establishment of the true values for the temperature at the onset of melt is of course very difficult because of problems discussed earlier dealing with the masking of the heated surface by the presence of carbon vapor or uncertainties in the interpretation of the radiant emission from the surface. In

the case of arc heated specimens the testing technique did not make it possible to provide a "black body" cavity for the optical sensor. As a result it was necessary to apply emissivity corrections to the brightness temperature ($\epsilon = 1.0$) results. In addition there is the concern that the presence of vapor may have also affected the recorded data. Examination of specimens that had "burned through" showed evidence of some vapor deposition at the edge of the resultant holes in the specimens, however, specimens that had not "burned through" did not exhibit any vapor deposit on the observed surface. On the basis of this, it seemed probable that while the back surface was still whole, that the gas flow over the rear surface prevented the migration of vapor into that zone and that vapor deposition occurred after the opening in the specimen.

For the arc tests therefore it was necessary to employ an emissivity correction to the results. From the spectrometer analysis employing Eqs. (4), (5), and (7) the dependence of temperature upon emissivity can be determined; this dependence is shown in Figures 32a and 32b. For a given wavelength and brightness temperature the parameter λT can be obtained from Figure 32a where upon the emissivity correction factor can be found in Figure 32b. Emissivity values employed for ATJ-S were obtained from References 16 and 17 where values for "graphite" are given and values for pyrolytic graphite were obtained from Reference 18. Spectrometer data it was stated were reduced, for spectral values between 2 and 4 microns yet the information on emissivity in those regimes is incomplete. From Reference 16 data is presented which suggest that an emissivity of 0.89 for graphite at 3900°K is applicable over the wavelength range from 0.25 to 1.8 microns. Since no other data was available in the literature that value was also chosen for the entire spectral range of the spectrometer results for ATJ-S. For pyrolytic graphite, establishing the rationale for the selection of emissivity was more difficult. In Reference 18 data are presented for ab-plane emissivity to 2.5 microns and for c-plane emissivity to 4.5 microns for temperatures up to 1780°C. C-plane emissivity for 1200°C shows a peak of around 0.92 at 1.0 micron and decreases to 0.76 at 4.5 microns while at 1780°C the peak is 0.8 at 1.0 micron with a decrease to 0.62 at 4.5 microns. The ab-plane emissivity at 1200°C is shown to peak at a value of 0.7 at 0.8 microns decreasing to 0.6 at 2.5 microns while at 1780°C it again peaks at 0.7 at 1.0 micron decreasing again to 0.6 at 2.5 microns. From these data one observes that the two curves (ab and c-plane) approach one another as temperature increases. Further it shows that the ab-plane peak emissivity remains unchanged and moves to higher wavelengths as temperature increases. With these trends no attempt was made to infer a spectral variation in emissivity at temperatures two thousand degrees higher than the available data. Rather a single value 0.7 was chosen. Since the back face of the pyrolytic graphite specimens was roughened due to machining and sanding, the value of 0.7 was picked as being an average between both c-plane and ab-plane behavior and a mean over the wavelength range.

Emissivity values determined as described above were employed to reduce the arc surface temperature data. Specimen temperatures were first obtained from the spectrometer data by averaging spectral brightness temperature values and then the corrections for emissivity were made to the average.

For the case of resistively heated specimens the same phenomena must be examined. In those tests vapor deposition was clearly evident after test in the region where the temperature of the material was being monitored. In the earlier discussion of those experiments it was suggested, based upon post test analyses and the examination of unfractured specimens, that vapor deposition probably occurred after melting. The validity of this hypothesis is difficult to establish, so that some question will remain as to whether the measured radiative intensities of the surface were attenuated by the presence of vapor. On the matter of emissivity, here too there has been some post test speculation. Although a cavity was provided for the purpose of making optical observations of the heated surface the diameter of the cavity that had to be employed because of the field of view limitations of the optical pyrometer resulted in an other than ideal "black body" cavity geometry. In fact the effectiveness of the cavity provided may have been negligible; the cavity did of course provide access to the high temperature zone of the specimen. It was concluded that an emissivity correction should also be made to the resistively heated specimens. The basis for selection of emissivity values for the resistance heated specimens follows from the data presented earlier from References 16, 17 and 18. Since the optical pyrometer employed in those tests operated in the 0.65 micron region, the emissivity value of 0.89 is appropriate for ATJ-S at that wavelength. After examining the emissivity curves for pyrolytic graphite at 0.65 microns for both ab and c-plane material one is led to the conclusion that the value of 0.7 used in the infra-red region is also the best value to use at 0.65 microns. Using these values the data were modified accordingly.

The modified phase diagram results are shown in Figure 33. The "corrected" temperatures show a shift of the solid-liquid boundary to higher temperature. An increase of approximately 150°K is exhibited at the triple point. The variation of the data with pressure is very insignificant although there appears to be a slight positive slope with increasing pressure. The primary effect exhibited in applying the temperature corrections was to change the relative location of the pyrolytic graphite data with respect to the ATJ-S. On the basis of brightness temperature the former indicates somewhat lower melt temperatures than the ATJ-S; when the corrections were employed the data show pyrolytic graphite indicating higher melting temperatures than ATJ-S. Obviously this shows a strong dependence on the emissivity factor. It is unfortunate that instrument limitations did not permit a smaller diameter cavity in the specimens for the resistively heated tests. This would have overcome the apparent emissivity uncertainty.

Examination of the data with respect to type of heating shows higher

temperatures were in general recorded in the arc tests. The effect of the gas environment does not appear to be discernable at least within the scatter of data. To attempt a closer examination on a point by point basis does not seem warranted in view of some of the uncertainties discussed.

The determination of the lowest pressure at which melting occurred (triple point) was made from the resistively heated specimens. By carefully controlling the pressure it was established in this study that the triple point was located at 102 atmospheres. The corresponding temperature for this pressure based upon the "corrected" resistively heated specimen data was determined to be 4100°K for both graphites. On the basis of the arc data however this temperature would be 4200°K for ATJ-S and approximately 4300°K for pyrolytic graphite. The variation in the behavior of the materials in the two heating environments can be attributed to a number of factors. Emissivity data quality is probably the primary influence on the results. As brought out in the report emissivity values for a nominal "graphite" material were also applied to ATJ-S and in so doing quantitative values had to be inferred for the appropriate spectral regions. Since the optical sensors used in the arc and resistance heater test environments operated in different spectral regions, small errors in emissivity could easily account for the 100°K difference in melt temperature indicated in Figure 30 for the two techniques. The emissivity uncertainty is more probable for the case of pyrolytic graphite since its emissivity is considerably lower than the black body value. The value of 0.7 chosen for both the visible and infra-red region of the spectrum was clearly a consensus of the data available with no attempt made to establish a spectral variation. It was felt that the extent of the available data did not warrant its extrapolation to establish a spectral dependence. Here again the potential error in emissivity values could easily explain the temperature difference (200°K) shown in Figure 33 for pyrolytic graphite in the two environments.

Another factor that had to be evaluated as a possible influence on the temperature measurements and more so for the resistance heating testing was the possible presence of vapor at the time of melt onset. After analyzing the data it was felt that the purge gas arrangement had been rather effective, however, there was considerable vapor deposited on the specimens at the conclusion of testing. While it was inferred that the deposition occurred after test, positive proof of this does not exist. The presence of vapor in the optical path would result in a decrease in measured temperature values.

Also shown in Figure 33 are results from Reference 6. The curve represents the solid-liquid boundary as established in that study for a nuclear grade graphite (LANG) determined using resistance heating. Comparison of that work with the data in this report shows the values of Reference 6 to be about 100°K higher than the ATJ-S data obtained resistively but in general agreement with the ATJ-S arc data. In view of the various factors discussed

that could have influenced the present results there does not appear to be any reason to explore further the slight difference between the results of Reference 6 and the present study.

F. Concluding Remarks

The experimental study described in this report was motivated to provide additional data on the melting of graphite which could assist in the resolution of apparent inconsistencies in existing results. Prior to this study data on melting had been obtained primarily from resistance heated specimens and was inferred from low pressure vaporization studies. The specific objective of the present work was to generate melting on externally heated specimens and compare these data with melting produced resistively. Experiments run in an arc heater did produce melted specimens whereas attempts with laser heating were unsuccessful. Using a resistance heater arrangement melted specimens were also generated for comparison purposes.

The major effort during the study was spent trying to generate an environment in which melting occurred on the external surface of a specimen in such a manner that the surface could still be observed to monitor its temperature. Whereas it was not too difficult to evolve an approach to heat the specimens to the melting temperature, it was extremely difficult to make an accurate measurement of surface temperature. The use of a scanning spectrometer with which to make surface radiation measurements from which to determine surface temperature initially seemed quite simple. It was hypothesized that optical "windows" would be available in the plasma and carbon vapor spectrum that specimen surface radiation could be observed. Because of the high pressure test environment, however, plasma radiation was intense. Not only were atomic lines and band systems present in these environments but continuum as well. This superposition of continuum plasma radiation over the continuum radiation of the specimen surface negated any chance of an accurate measurement of specimen surface temperature. To overcome this problem it became necessary to observe the test specimens from the back face. Unfortunately this eliminated any chance of sensing changes in radiation intensity as influenced by changes in surface reflectivity produced by phase change from the solid to the liquid. Although the problem was acute with the spectrometer operating in the infrared spectrum, it would not have been much better if the instrument were modified to operate in the visible or ultra-violet.

Another problem area that became apparent in the study for both the arc heated and resistance heated testing was that of material emissivity. In the arc testing since the heating was applied on the front face it was not possible to employ a black body cavity within which to measure material temperature. This necessitated the use of emissivity corrections to the brightness temperature data and since such data are sparse, some uncertainty in the reduced temperature values follows. The problem of emissivity was

much more complex with the pyrolytic graphite material because of its lower emissivity values and the greater spectral dependence of the data.

Emissivity also became a problem in interpreting resistance heated specimen results. Because of optical instrument limitations the viewing cavity in the specimens was increased sufficiently to nullify the effectiveness of the cavity as a black body opening. Here again the problem was more severe with the pyrolytic graphite material than with the ATJ-S graphite. In view of this it would appear that in any future work a material such as pyrolytic graphite not be used; a better candidate would be purified ATJ material.

Considering the problem of carbon vapor and its effect on the results, in general it is felt that the purging technique employed was rather successful. Although vapor deposition was observed in both types of heating experiments at the end of a test when the hardware was disassembled, it seems highly probable that during testing the presence of vapor in the optical path was negligible and did not affect the measurements. The utility of the guard heater in eliminating vapor condensation in the resistance heating tests appears to have been masked by the extension of the purge gas tube up to the immediate proximity of the test specimen cavity. However, the guard heater did assist in minimizing specimen heat transfer losses. Although guard heater effectiveness could be explored in any subsequent investigation, the purge gas arrangement employed may be more effective.

In summary, the experimental study that was conducted produced additional data employing both external heating (arc) and internal heating (resistance) techniques to determine the melting behavior of graphite. While there are certain reservations in the interpretation of the data, the results as such do not indicate any large differences from data previously obtained by other investigators such as Schoessow 8. Because of various experimental difficulties the scatter in the melt temperature values especially for externally heated specimens was greater than expected, however, before better measurements can be made in the high pressure environments improved instrumentation techniques must be evolved.

SECTION VIII

REFERENCES

1. Basset, J.M., J. Phys. Radium 10, 217-228 (1939).
2. Steinle H. Z., Angew Mineral 2, 344 (1940)
3. Jones, M. T., Summary Report PRC-3, National Carbon Research Labs., Parma, Ohio, January 1958.
4. Noda, T., Proceedings of the International Symposium on High Temperature Technology, Stanford Research Institute, 1959.
Published by McGraw-Hill, New York, 1959.
5. Fateeva, N. S., Vereshchagin, L. F. and Koiotygin, V. A., Soviet Physics-Doklady, 8, 893 (1964).
6. Schoessow, G. J., "Graphite Triple Point and Solidus-Liquids Interface Experimentally Determined Up To 1000 Atmospheres", Report prepared under Contract No. NAS 3-010412 by University of Florida, Gainesville, Florida, December 1967.
7. Drowart, J., Burns, R. P., DeMaria, G., and Inghram, M. G., J. Chem. Phys. 31 1131 (1959).
8. "Vapor Pressure of Carbon", The Industrial Graphite Engineering Handbook, Union Carbide Corp., 1965, p. 5B.06.05.
9. Zavitsanos, P. D., General Electric Rpt. No. R66SD31, Space Sciences Laboratory, May 1966.
10. Marston, C. H., Frind, G., Michkovsky, V. and Schorn, A. M., "Research Study of Radiation Heat Flux from High Pressure Air Arcs", AEDC TR-66-258, December 1966.
11. Martin, M., Private Communication.
12. Scarborough, J. B., Numerical Mathematical Analysis, (5th ed.), The Johns Hopkins Press, Baltimore, 1962.

13. Brandkamp, W., Private Communication
14. Bundy, F. P., "Melting of Graphite at Very High Pressure",
J. Chem. Phys. 38, (1963).
15. Stover, E. R. and Magin III, F. P., "Microstructure of Graphite
Formed by Growth from the Liquid or Vapor at High Pressures",
Unpublished Studies at GE-RESO, 1969.
16. The Industrial Graphite Engineering Handbook, Union Carbide Corp.,
N. Y., (1964).
17. Mantell, C. L., Carbon and Graphite Handbook, Interscience
Publishers, John Wiley & Sons, New York, N. Y., 1968.
18. Pyrolytic Graphite Engineering Handbook, Metallurgical Prod.
Dept., General Electric Company, 1964.

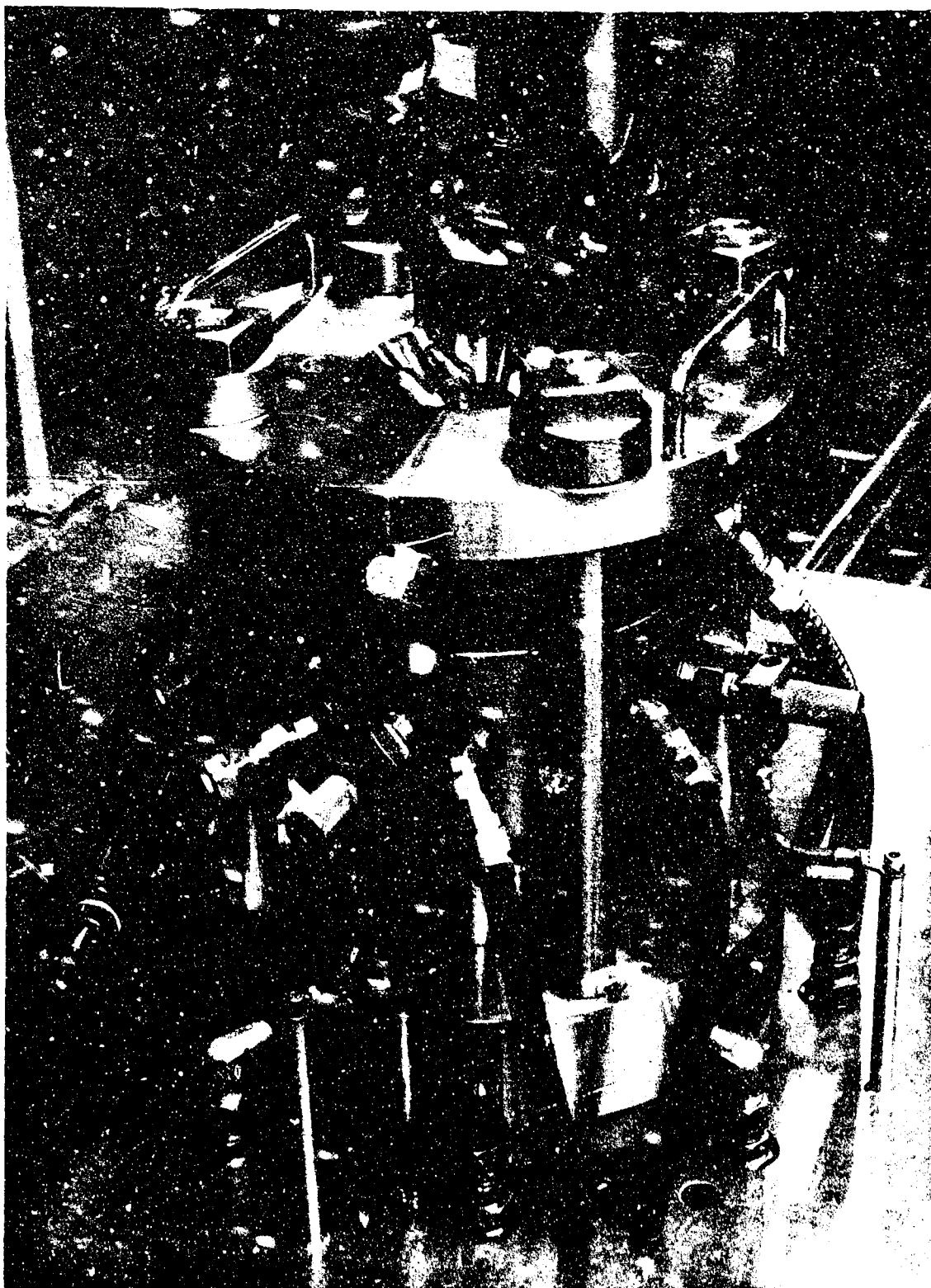


FIGURE 1a HIGH PRESSURE ARC, MK II

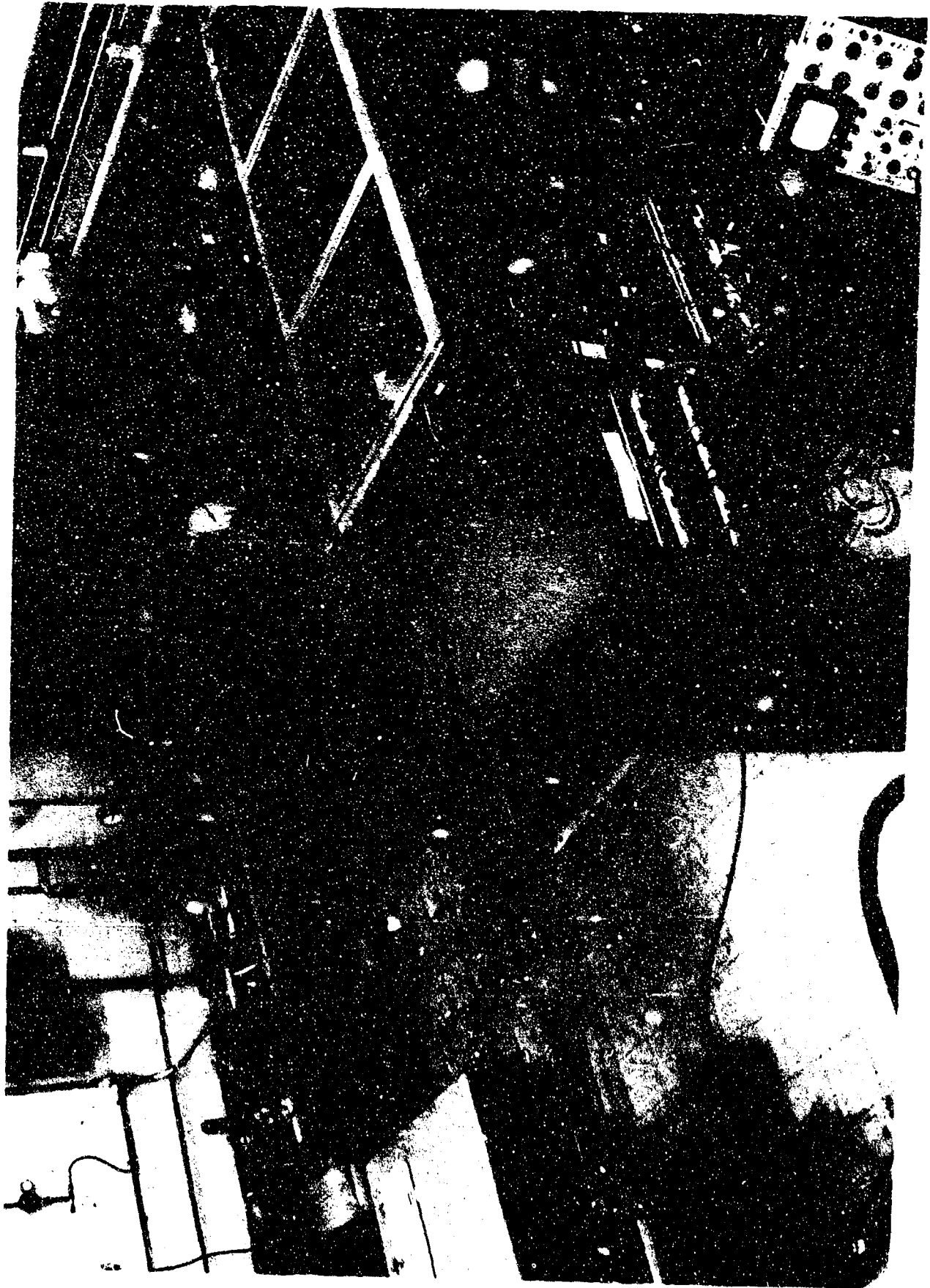


FIGURE 1b TEST ARRANGEMENT FOR ARC HEATING OF GRAPHITE SPECIMENS



FIGURE 2 PULSED LASER USED FOR SPECIMEN HEATING

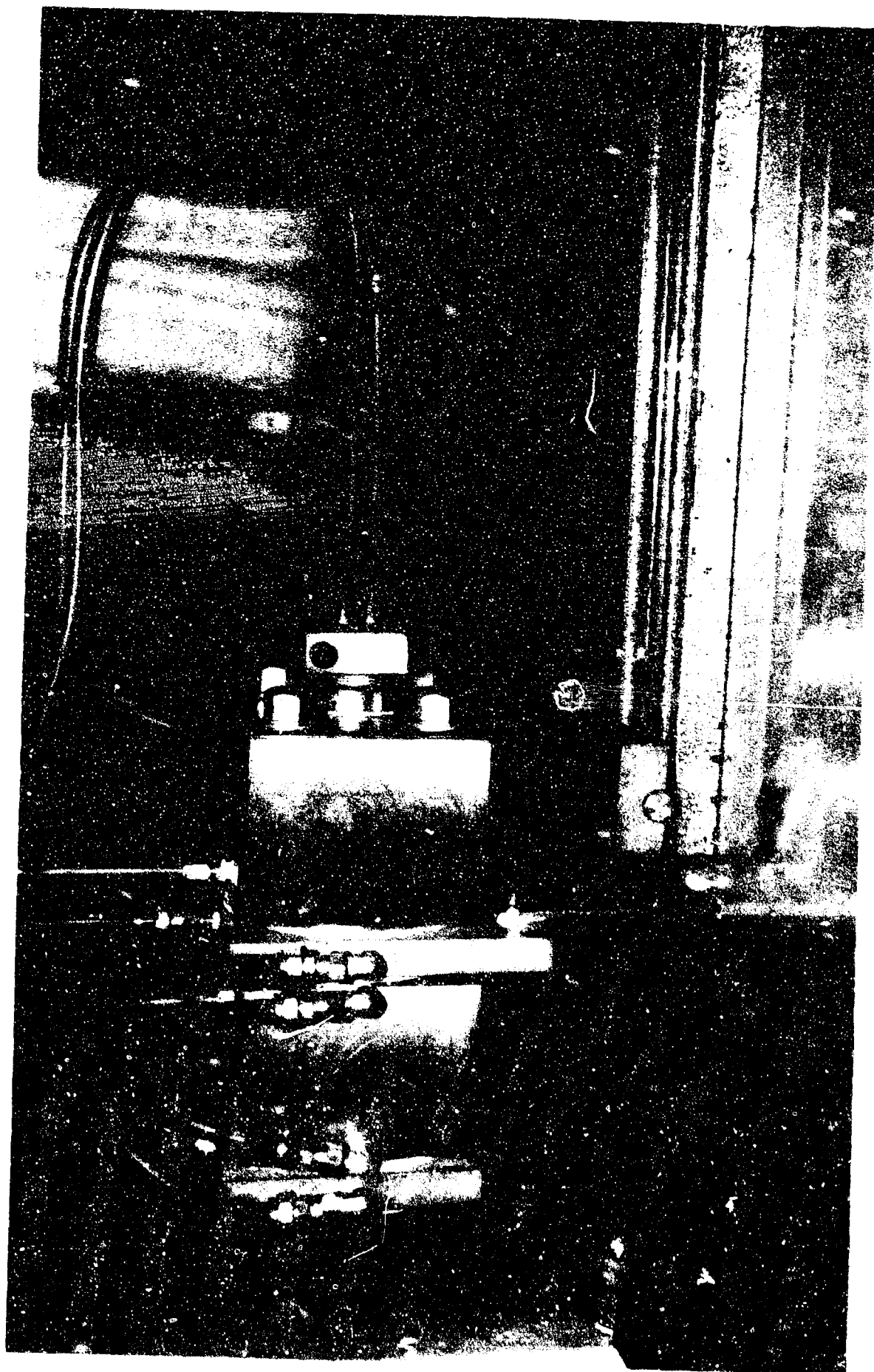
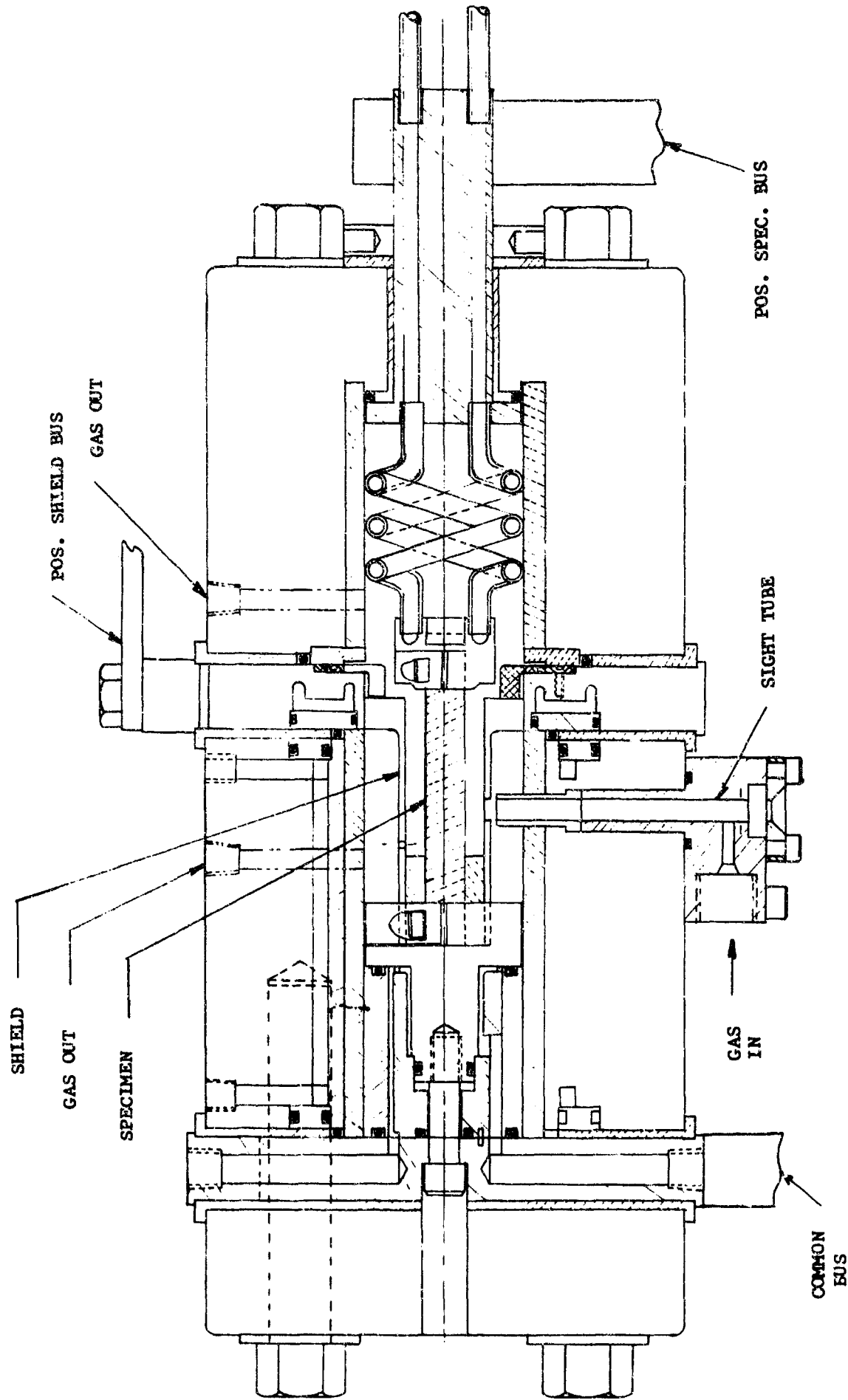


FIGURE 3a RESISTIVE HEATER ASSEMBLY



38

FIGURE 3b RESISTIVE HEATING EXPERIMENTAL APPARATUS

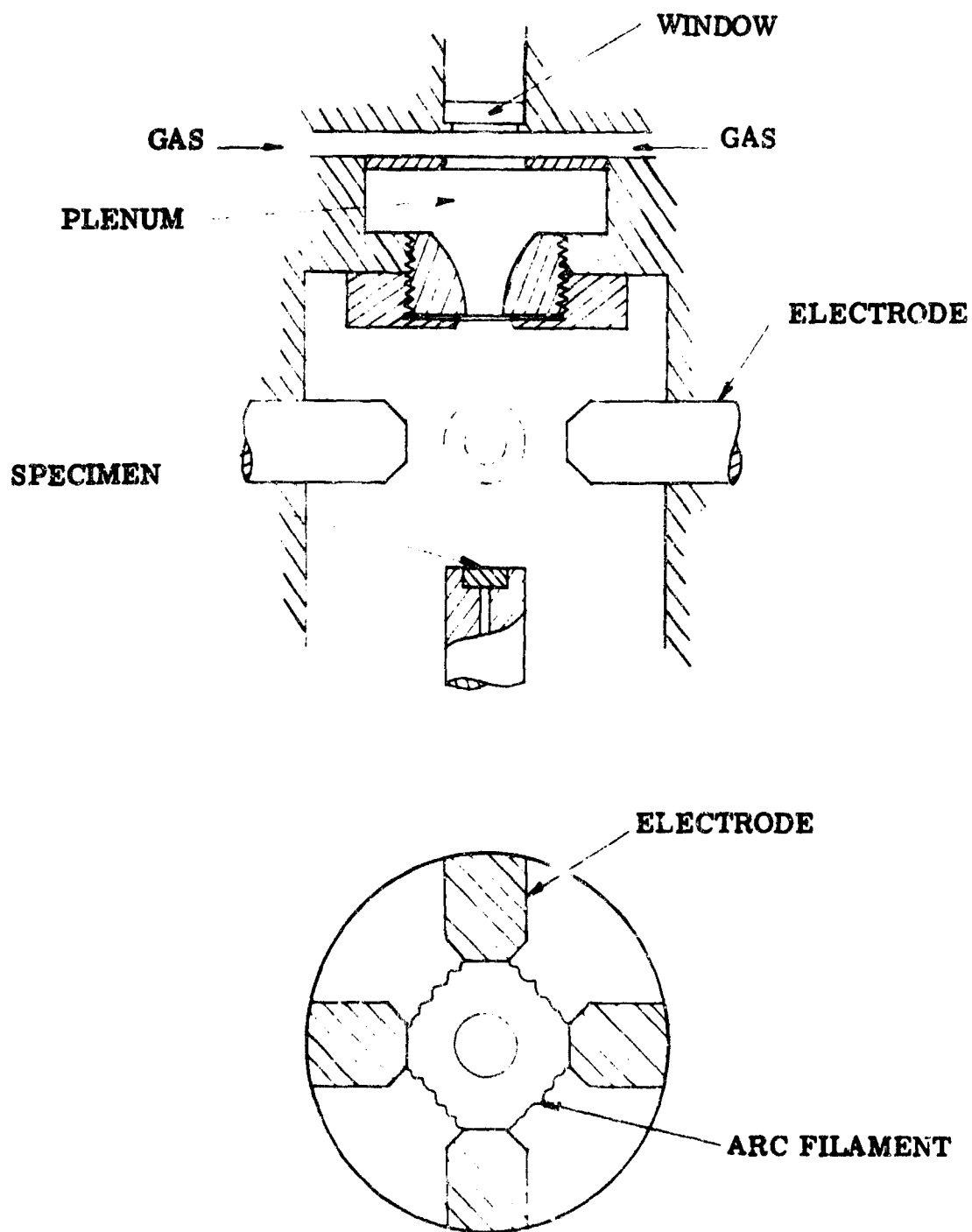


FIGURE 4 SKETCH OF MK II ARC HEATER ELECTRODE ARRANGEMENT

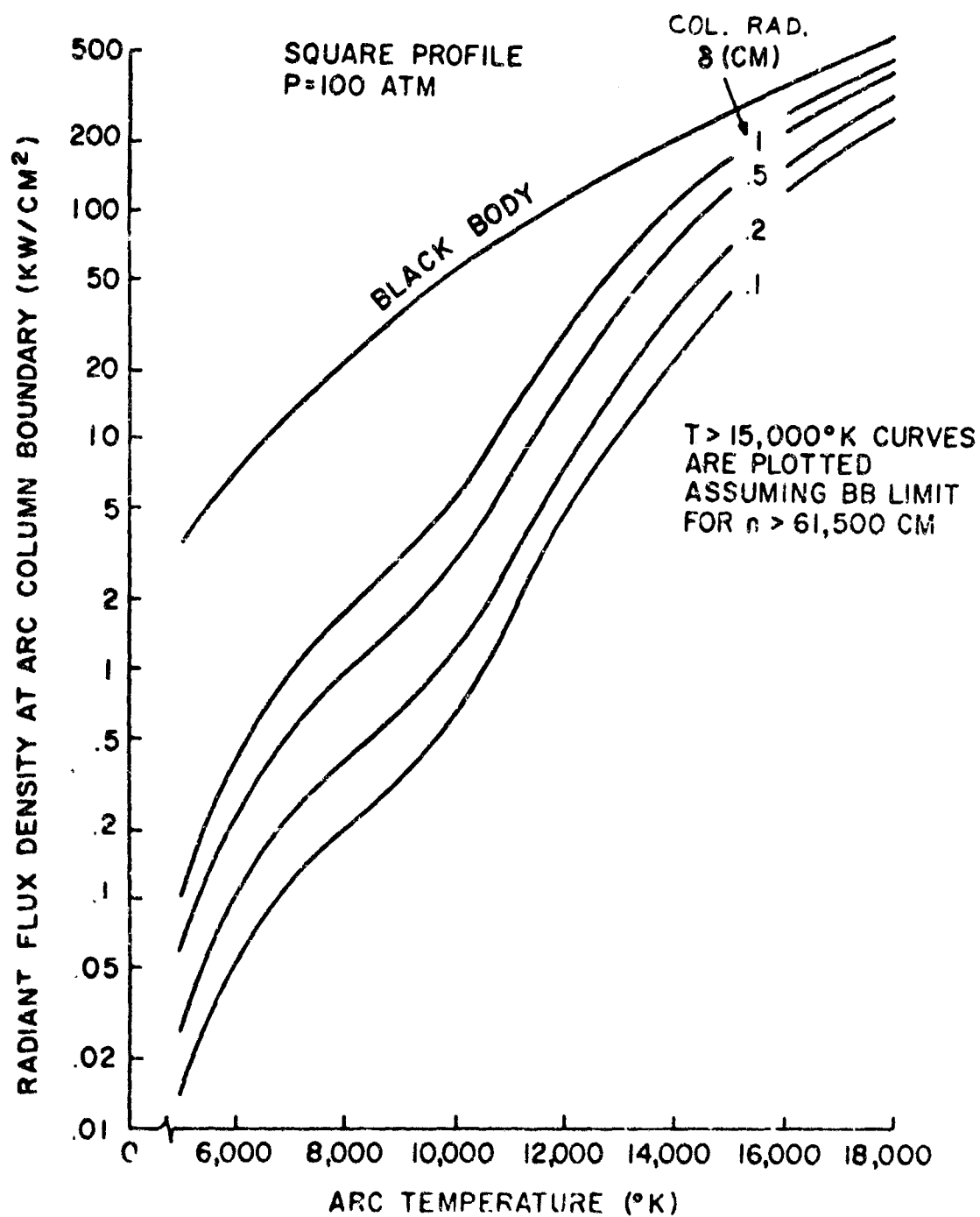


FIGURE 5 ARC COLUMN RADIANT INTENSITY AT 100 ATMOSPHERES
PRESSURE (REF. 10)

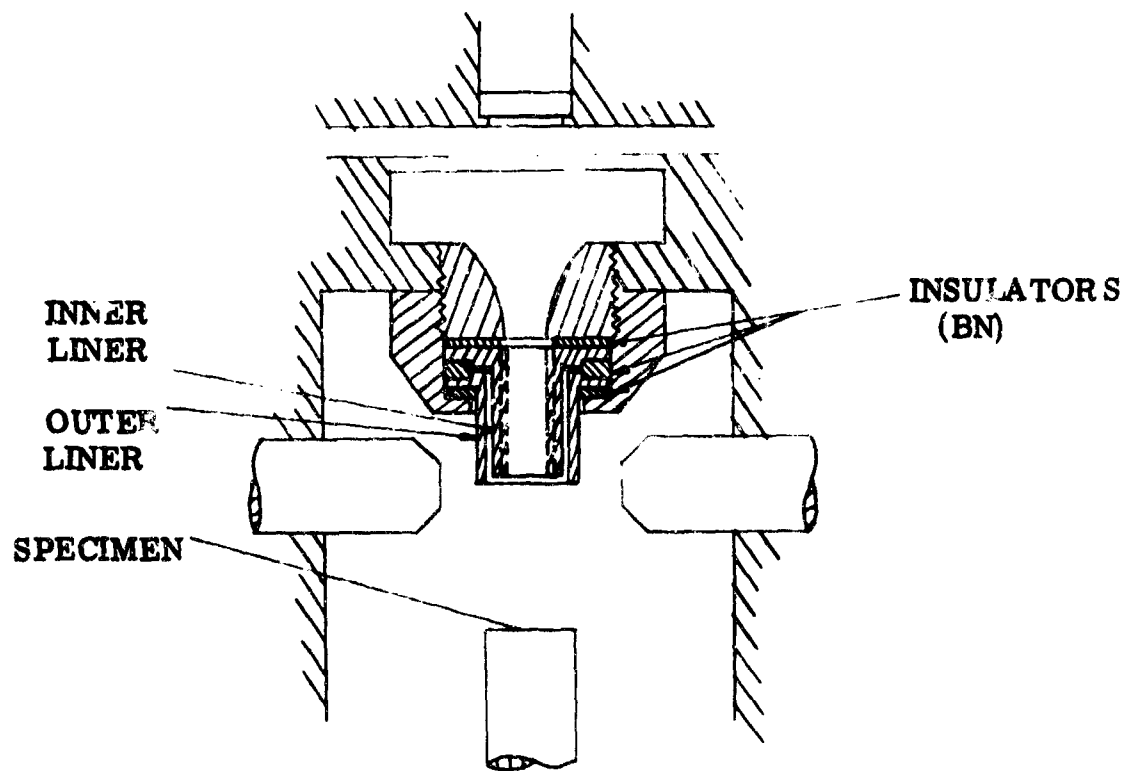


FIGURE 6 GAS INLET TUBE ADAPTER FOR ARC HEATER

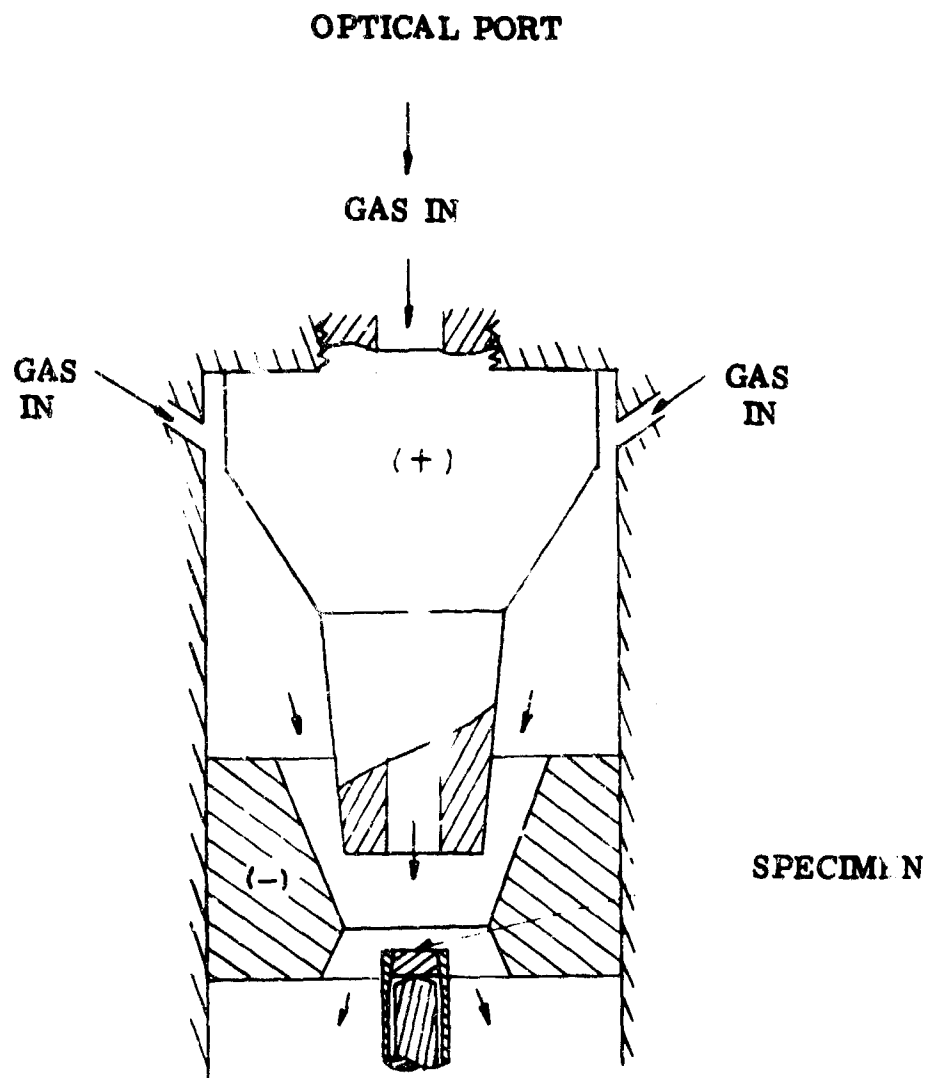


FIGURE 7 MODIFIED ELECTRODE ARRANGEMENT FOR ARC HEATER

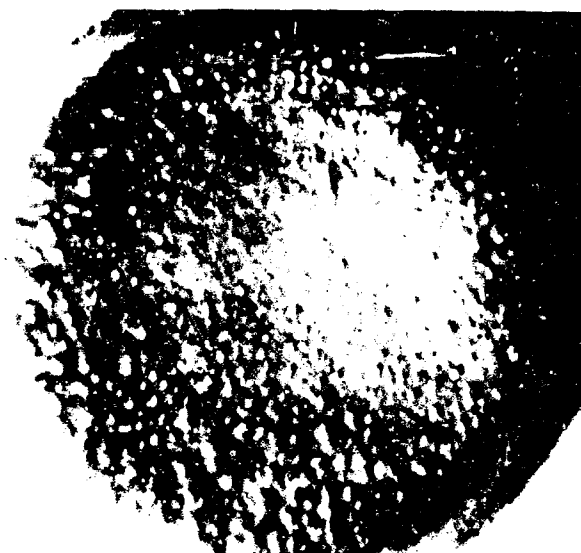


FIGURE 8 ARC HEATED PYROLYTIC GRAPHITE SPECIMEN SHOWING
SOLIDIFIED NODULES ON SURFACE, AT 7X AND 149 ATM
IN ARGON

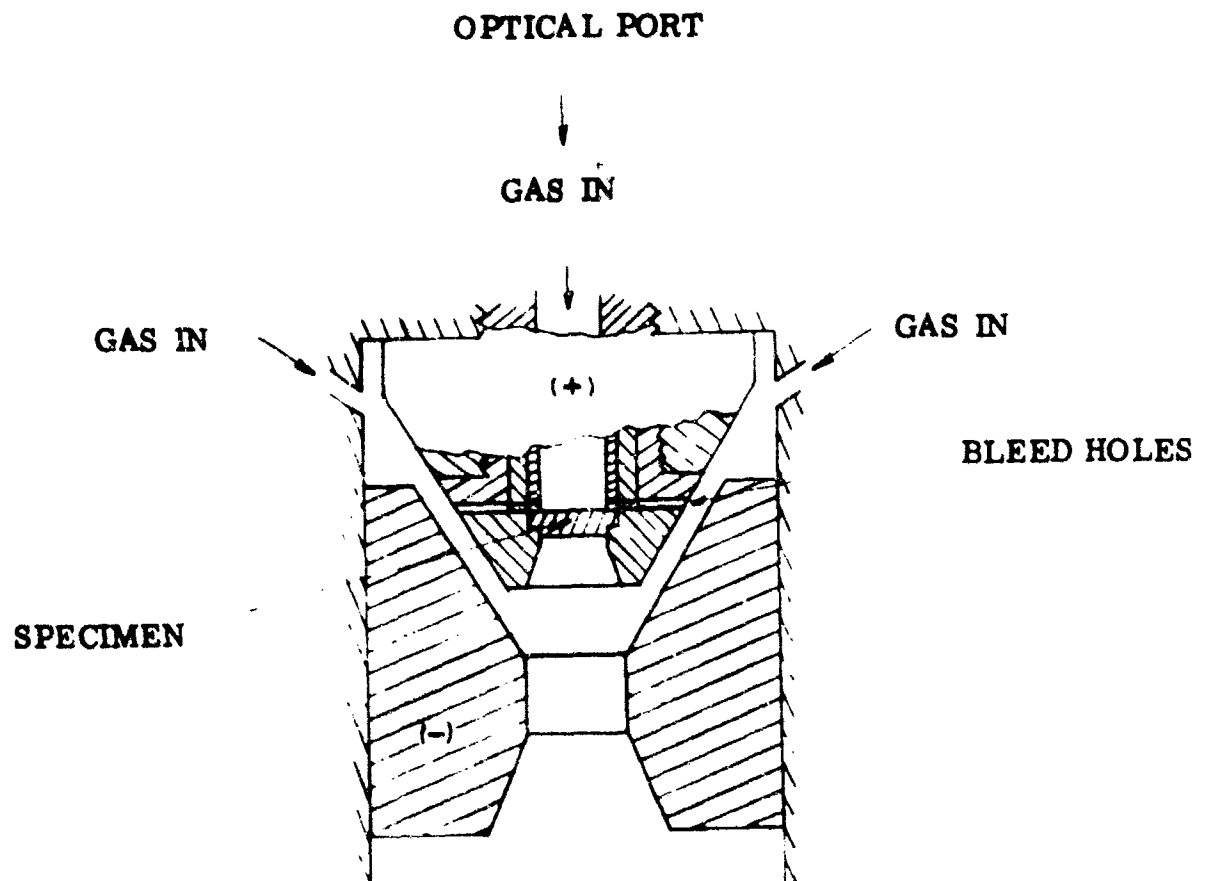


FIGURE 9 FINAL TEST SPECIMEN ARRANGEMENT - ARC HEATER

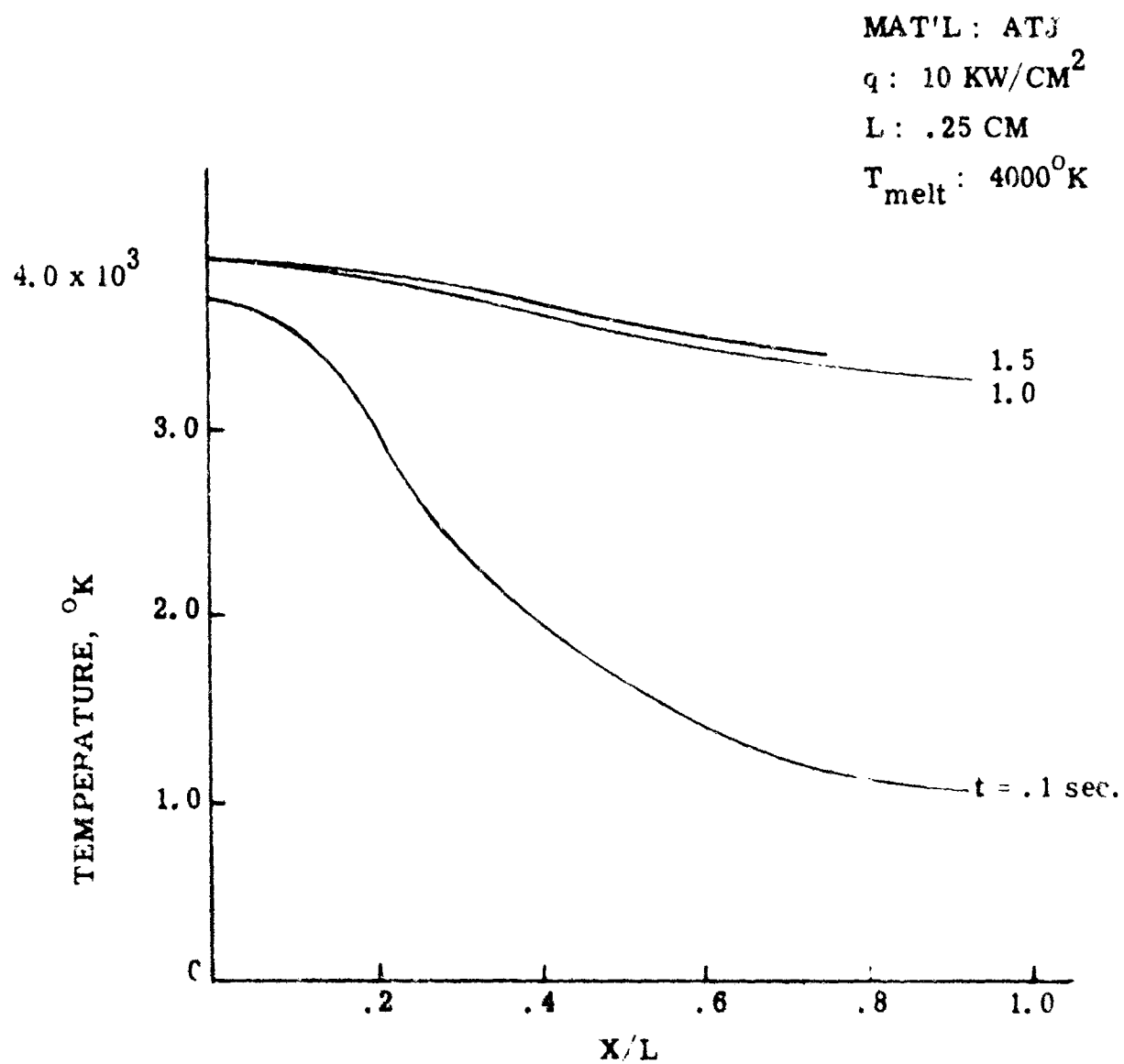


FIGURE 10 TEMPERATURE DISTRIBUTION IN ATJ SPECIMEN

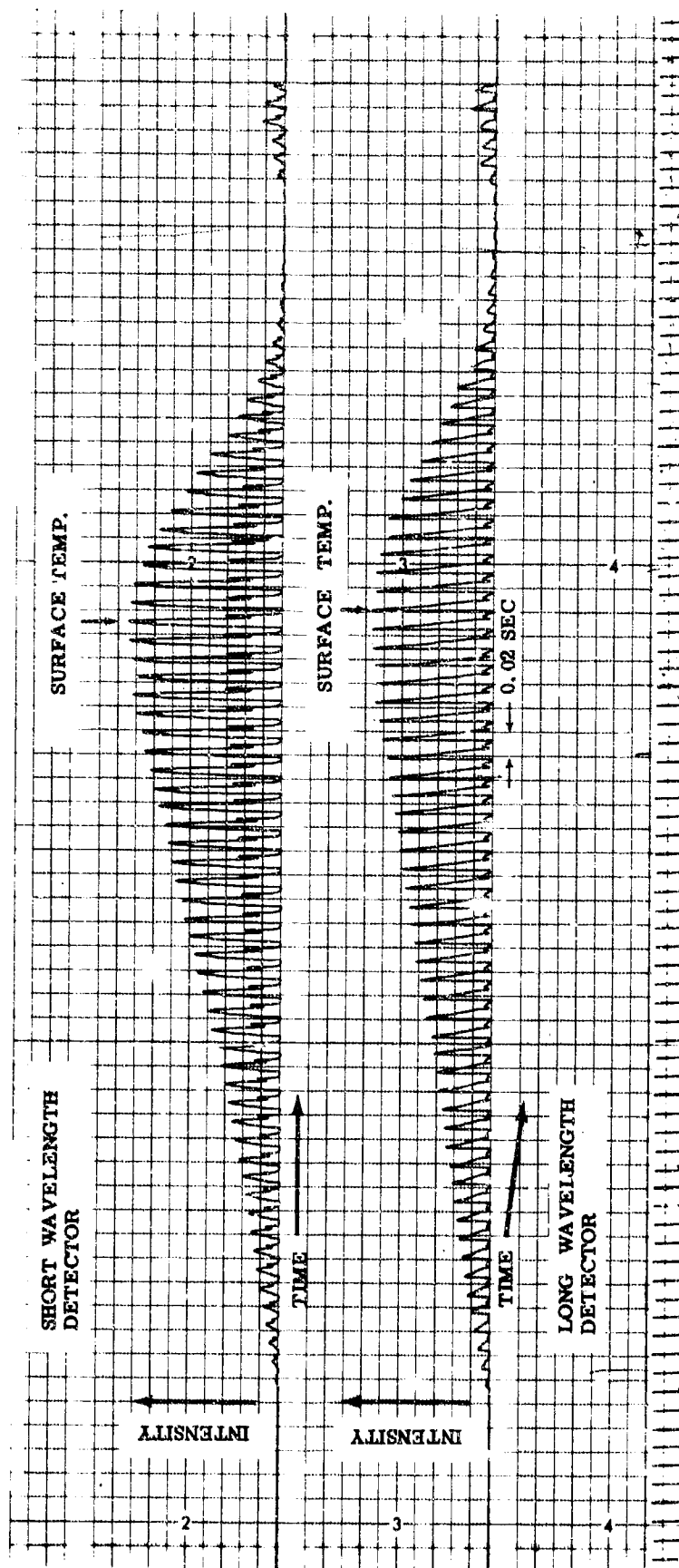


FIGURE 11 SPECTROMETER ANALOGUE DETECTOR OUTPUTS



FIGURE 12 ARC HEATED PYROLYTIC GRAPHITE SPECIMEN
AFTER TEST SHOWING RECESSION OF FRONT
SURFACE THROUGH TO BACK SURFACE, AT
2X AND 153 ATM IN NITROGEN

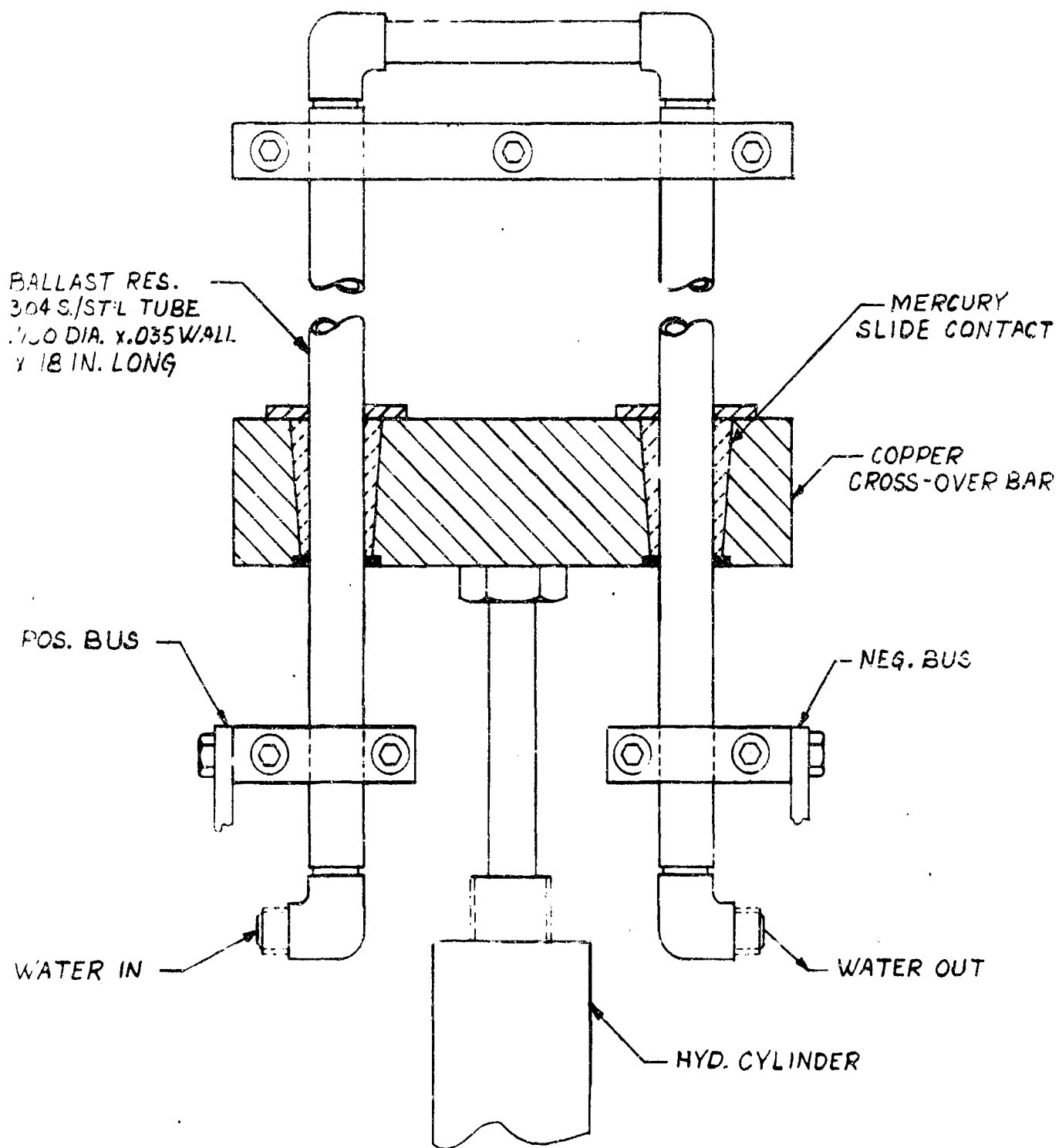


FIGURE 13 BALLAST RESISTOR FOR RESISTANCE HEATER

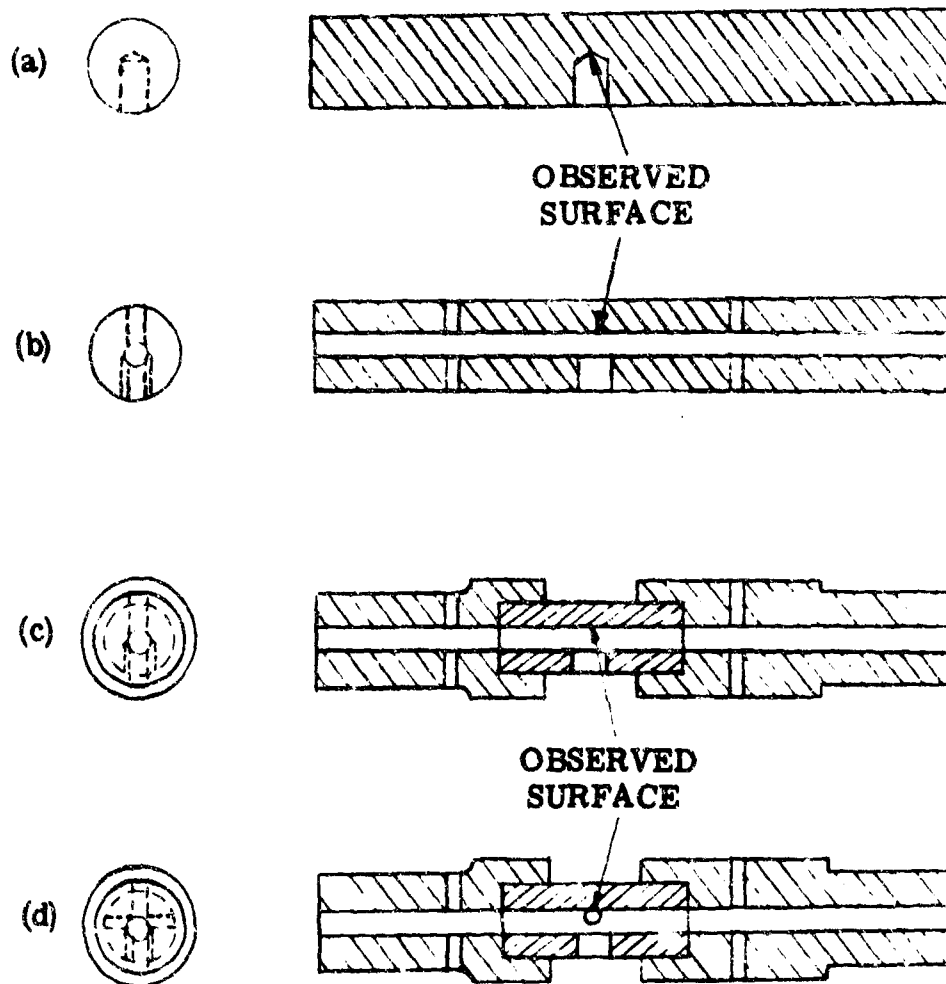
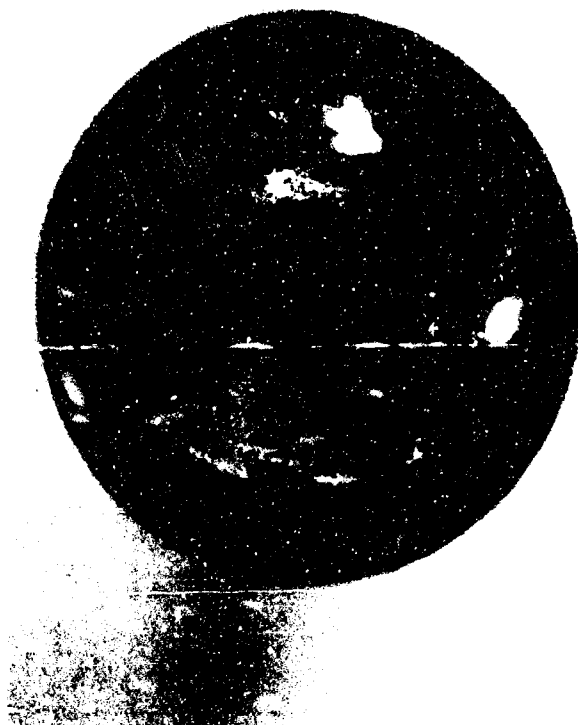


FIGURE 14 RESISTANCE HEATER SPECIMEN CONFIGURATIONS



**FIGURE 15 SECTIONED ATJ-S SPECIMEN AFTER RESISTANCE
HEATING SHOWING SOLIDIFIED INTERIOR AND
EXPANDED CROSSECTION AT 5.5X AND 135 ATM
IN ARGON**



**FIGURE 16 TYPICAL RESISTANCE HEATED SPECIMEN AFTER
TEST SHOWING SOLIDIFIED GRAPHITE, AT 5.5X
P = 238 ATM**

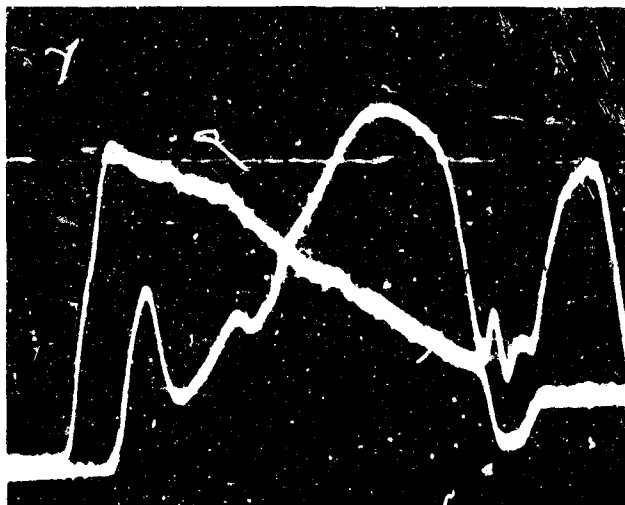


FIGURE 17 SHORT AND LONG WAVELENGTH
SPECTROMETER SCANS
(BLACK BODY at 1273°K)

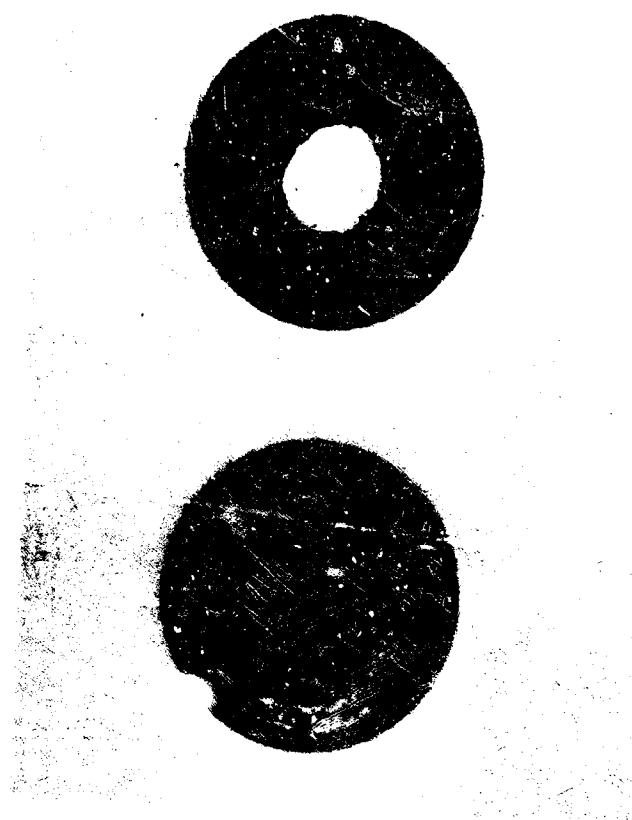


FIGURE 18 ATJ-S SPECIMENS HEATED IN NITROGEN
ENVIRONMENT IN ARC HEATER
P = 164 & 144 ATM (3. 3X)



FIGURE 19 PYROLYTIC GRAPHITE SPECIMEN HEATED
IN NITROGEN ENVIRONMENT IN ARC HEATER
P = 164 ATM (3.3X)



FIGURE 20 POLISHED SECTION OF DROP COLLECTED FROM GRAPHITE
SAMPLE RESISTANCE HEATED TO HIGH PRESSURE, SHOWING
"COLLAPSED" FORM AND CRYSTALS IN THE VICINITY OF THE
BUCKLED SIDE; LEFT: 30 X; RIGHT, 100 X.
P = 203 KTM, NITROGEN GAS



FIGURE 21 CRYSTALS IN SOLIDIFIED DROP SHOWN IN FIGURE 20, PHOTOGRAPHED AT 860 X WITH OIL IMMERSION LENS IN POLARIZED LIGHT; TOP: TWO REGIONS NEAR SURFACE OF DROP; BOTTOM: REGIONS FROM CENTER OF DROP SHOWING DIFFERENCES IN CRYSTAL SIZE



FIGURE 22

SECTION THROUGH WALL OF ATJ-S RESISTIVELY HEATED AT 238 A°M; 50 X IN POLARIZED LIGHT. OUTSIDE DIAMETER, AT LEFT, SHOWS A THIN LAYER OF FINE VAPOR-DEPOSITED CRYSTALS AND REMNANT OF LIQUID TO TOP OF THE WALL. INSIDE DIAMETER SURFACE, AT RIGHT, SHOWS A THICKER LAYER OF FINE VAPOR DEPOSITED CRYSTALS. FORM OF SOLIDIFIED DROPLET SUGGESTS A LARGE SHRINKAGE; NOTE UNIFORM CONCAVE INTERFACE WITH UNMELTED MATERIAL AT BOTTOM. NOTE ALSO THE CONTACT ANGLE AT RIGHT, TYPICAL OF SOLIDIFIED DROPS IN THESE EXPERIMENTS. DARK CAVITY IN CENTER OF FIELD WAS PROBABLY CREATED BY PULL-OUT OF A LARGE PLATE PARALLEL TO THE FIELD OF VIEW DURING MICROPOLISHING. (ARGON GAS)



FIGURE 23 VIEWS OF FIGURE 22 AT 860 X IN POLARIZED LIGHT, SHOWING TOP OF LEFT (OUTER) WALL, AT TOP, AND SECTION THROUGH INNER WALL WITH THICK LAYER OF VAPOR DEPOSIT, AT RIGHT.



FIGURE 24 VIEW OF FIGURE 22 AT 860 X IN POLARIZED LIGHT, SHOWING GRA PHITE CRYSTALS ORIENTED PARALLEL TO THE SURFACE OF THE COLLAPSED, SOLIDIFIED DROP; NOTE REGION AT LEFT CONTAINING REGION OF SMALLER CRYSTALS SIMILAR TO THOSE ON THE INNER WALL SURFACES NEXT TO THE LIQUID IN FIGURE 23. AREA IS AT EXACT CENTER OF FIGURE 22.



FIGURE 25a VIEW OF FIGURE 22 AT 860 X IN POLARIZED LIGHT, SHOWING UNMELTED ATJ-S, AT LEFT, AND COLUMNAR GRAINS WHICH GREW FROM THE SOLID INTO THE LIQUID DURING SOLIDIFICATION; MANY INTERPLANAR CRACKS HAVE OPENED DUE TO THE ANISOTROPIC CONTRACTION OF THE GRAPHITE CRYSTALS ON COOLING TO ROOM TEMPERATURE.



FIGURE 25b CONTINUATION OF FIGURE 25a, 860 X IN POLARIZED LIGHT, SHOWING INTERFACE BETWEEN COLUMNAR SOLIDIFIED MATERIAL, AT LEFT, AND CRYSTALS SOLIDIFIED FROM REMAINDER OF THE LIQUID TO SURFACE OF DROP AT RIGHT.

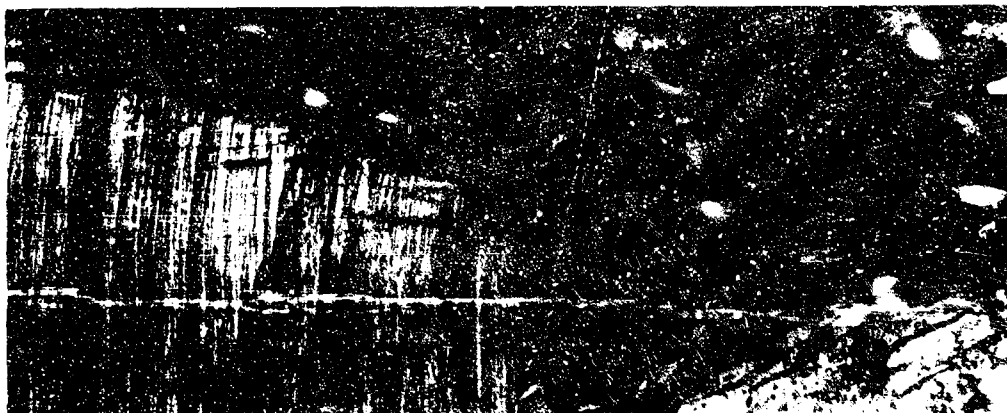


FIGURE 26 ARC-HEATED PYROLYTIC GRAPHITE SHOWING DROPLET FORMED AT 157 ATM; LEFT: 100 X; RIGHT: 860 X. NOTE TENDENCY OF CRYSTAL GROWING FROM THE SURFACE TO ORIENT PARALLEL TO THE PYROLYTIC GRAPHITE PLANES. (ARGON GAS)

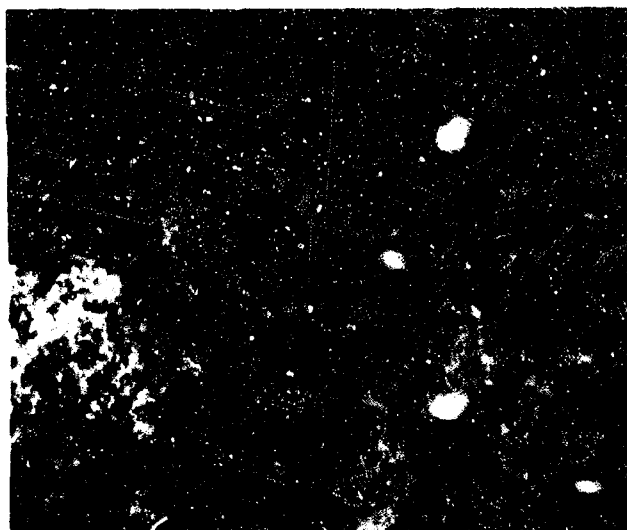


FIGURE 27 ARC-HEATED ATJ-S SHOWING DROPLET FORMED AT 167 ATM, AT 500 X (ARGON GAS)



FIGURE 28 APPEARANCE OF GRAPHITE CRYSTALS ON THE SURFACE
(LEFT) AND WITHIN A GRAPHITE DROPLET (RIGHT) AS SHOWN
BY SCANNING ELECTRON MICROSCOPY. 2000 X.

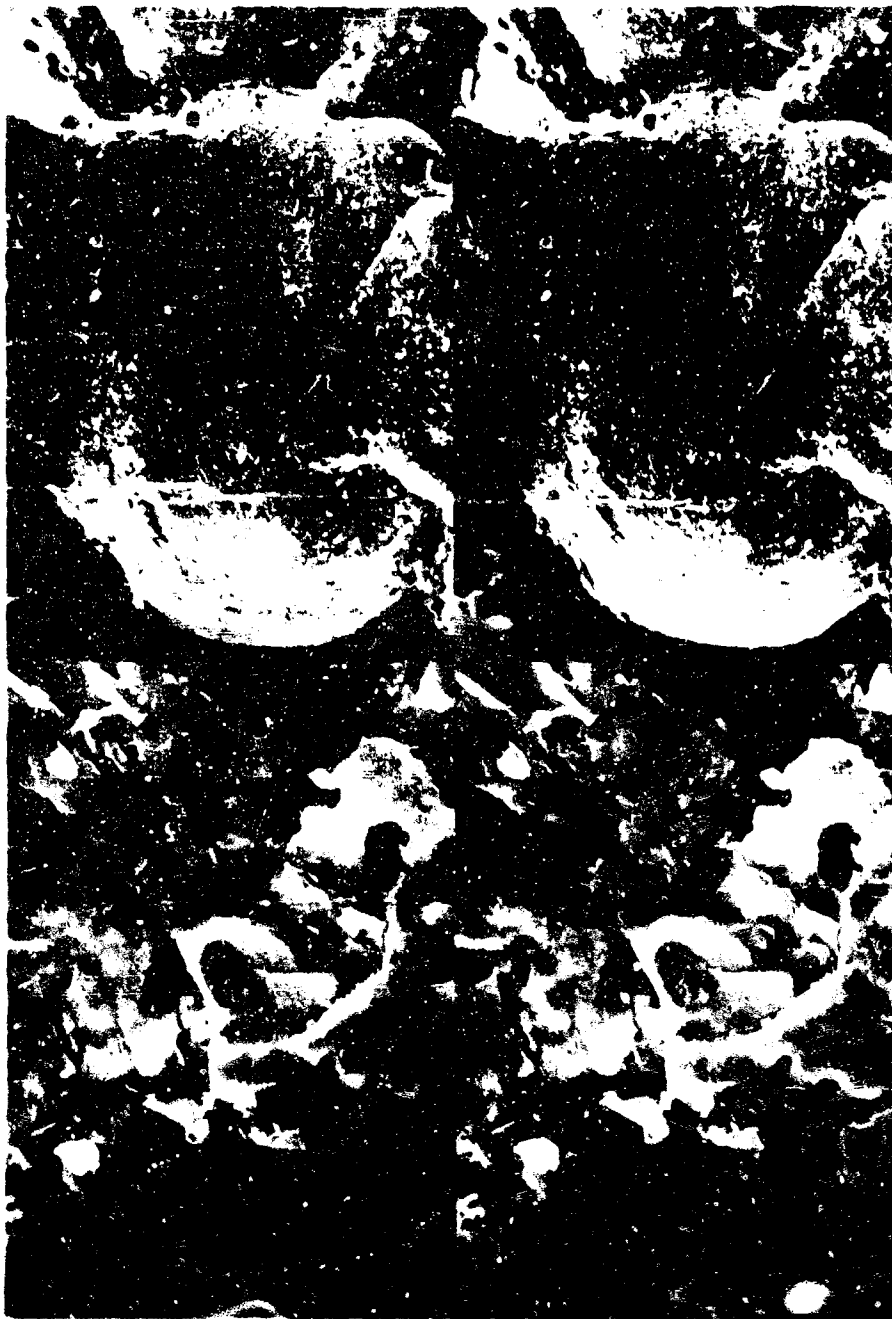


FIGURE 29 STEREOSCOPIC VIEWS OF A GRAPHITE DROPLET
SHOWING SURFACE ORIENTATION OF GRAPHITE
CRYSTALS; TOP: 20 X; BOTTOM: 500 X.



**FIGURE 30 STEREOSCOPIC VIEWS OF SAME GRAPHITE DROP
SHOWN IN FIGURE 29 AFTER SECTIONING WITH A
BLADE: TOP: 20 X; BOTTOM: 500 X.**

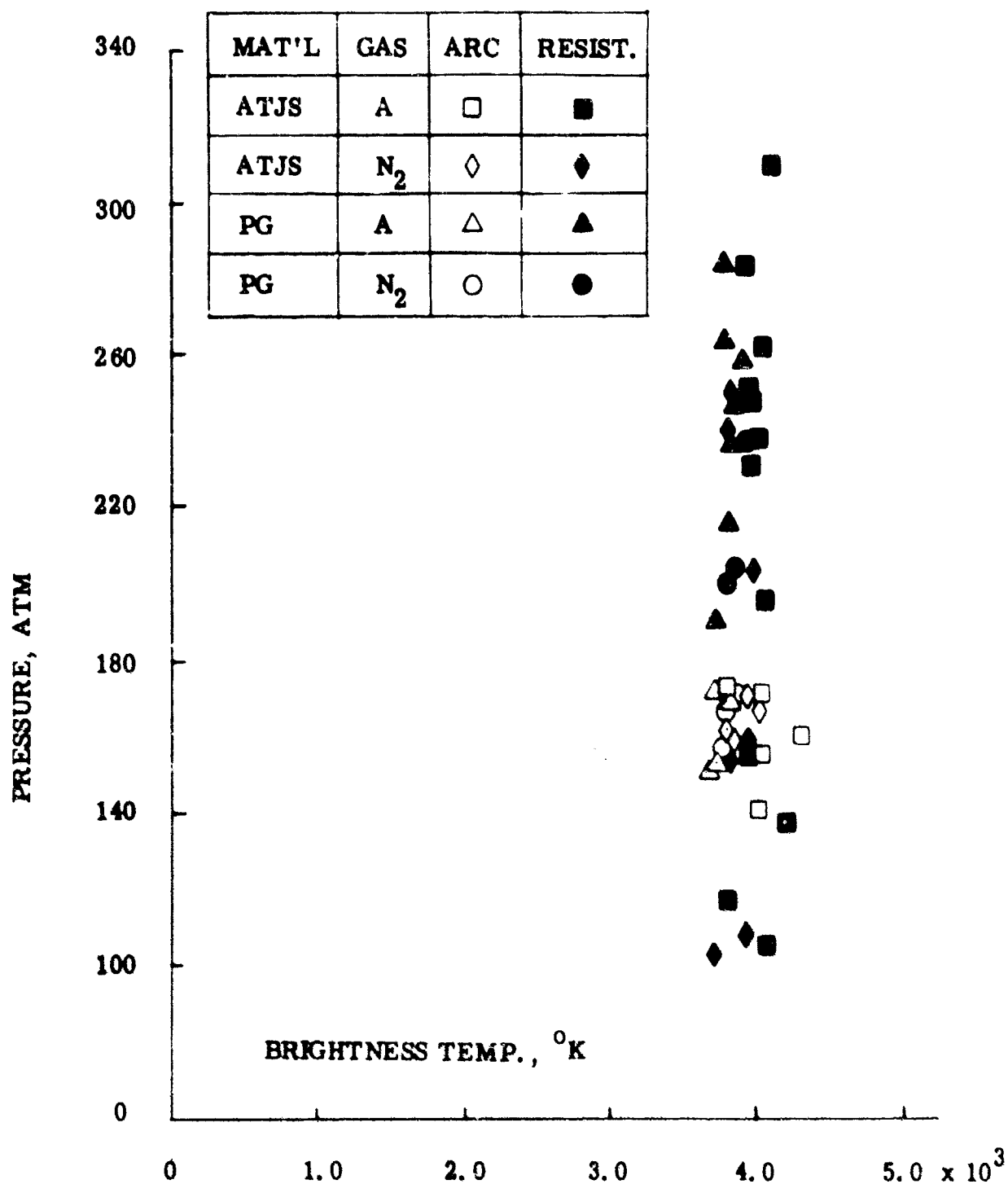


FIGURE 31 GRAPHITE PHASE DIAGRAM

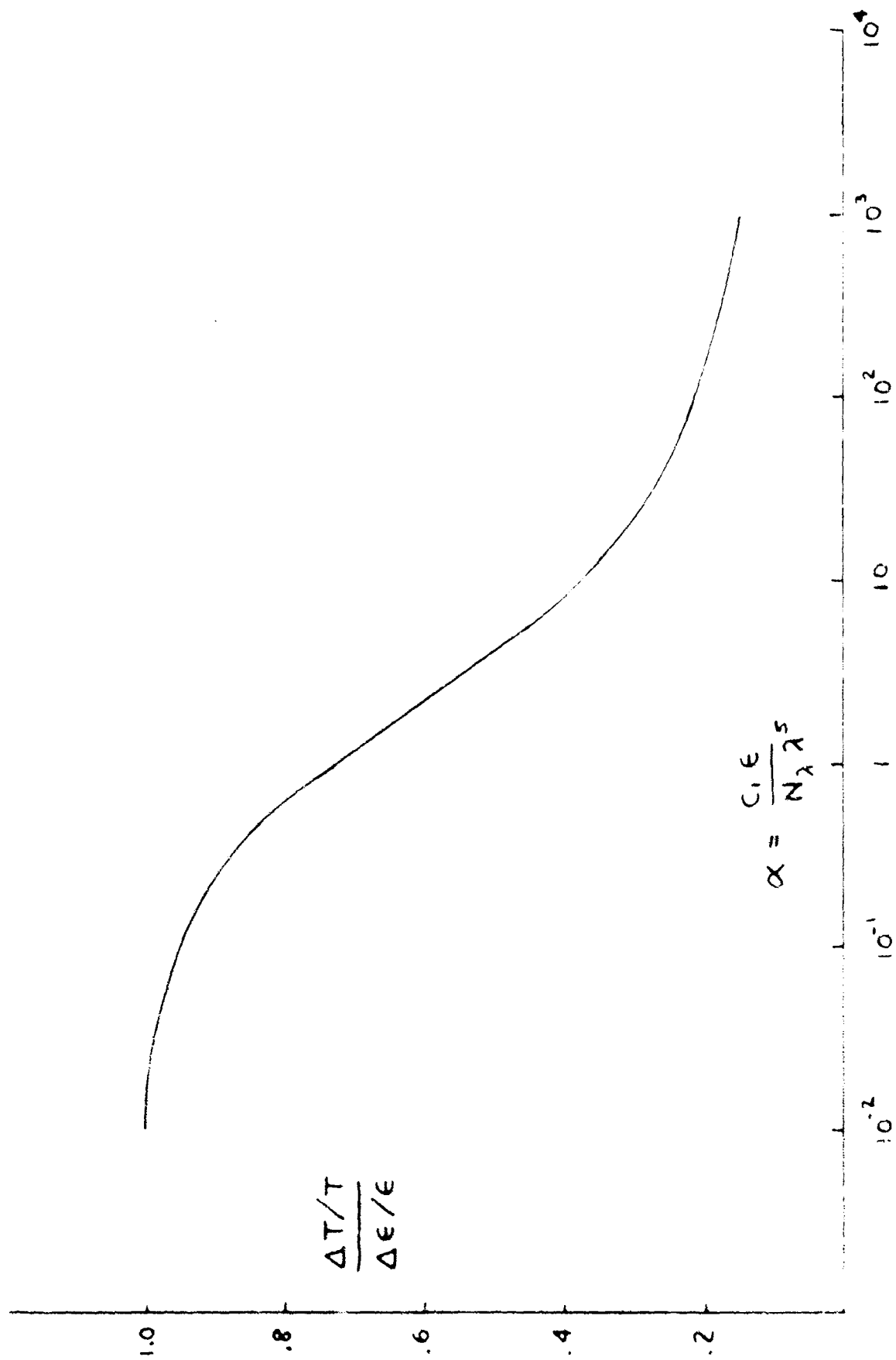


FIGURE 32a EMISSIVITY FACTORS FOR SCANNING SPECTROMETER DATA

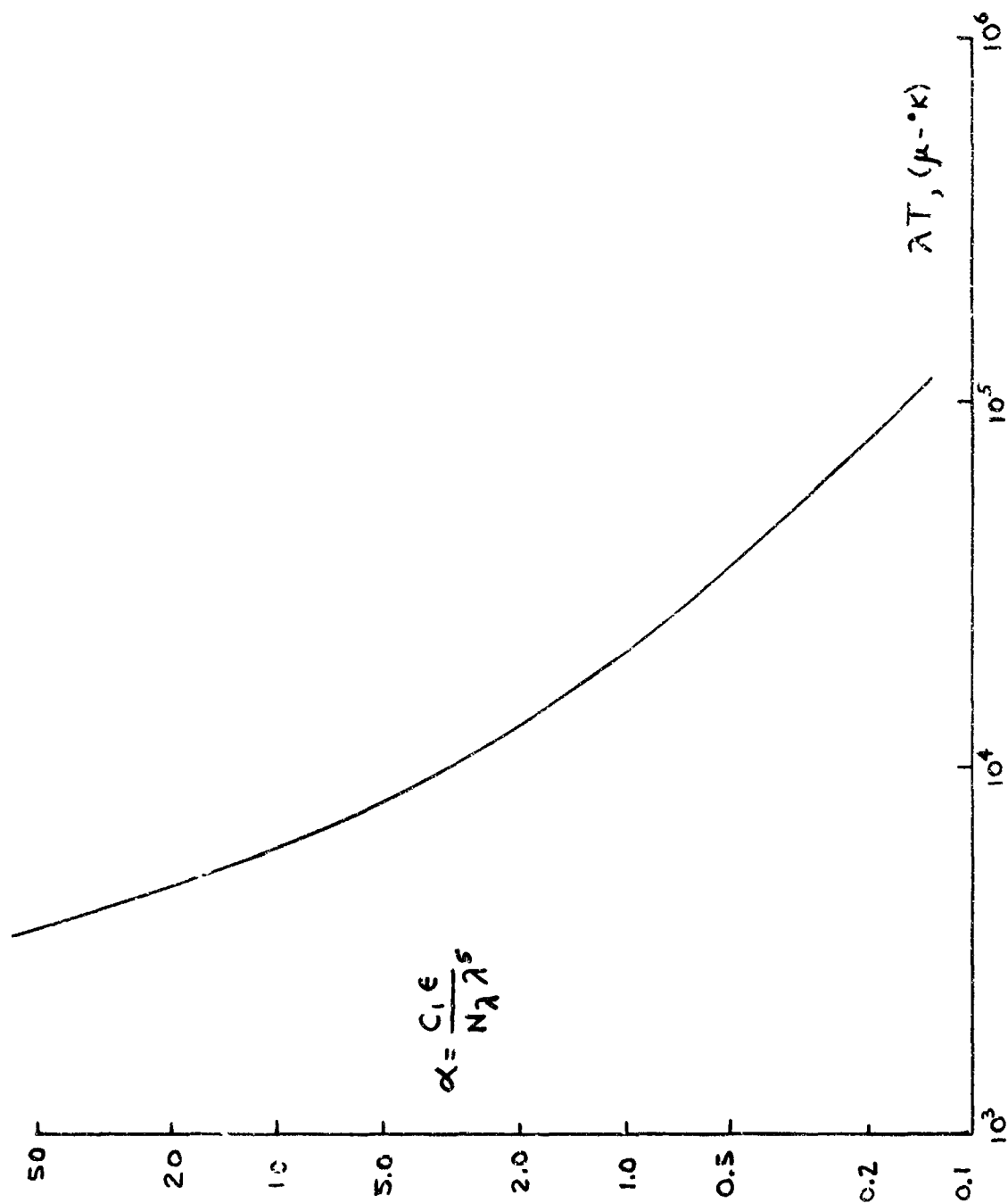


FIGURE 32b EMISSIVITY FACTORS FOR SCANNING SPECTROMETER DATA

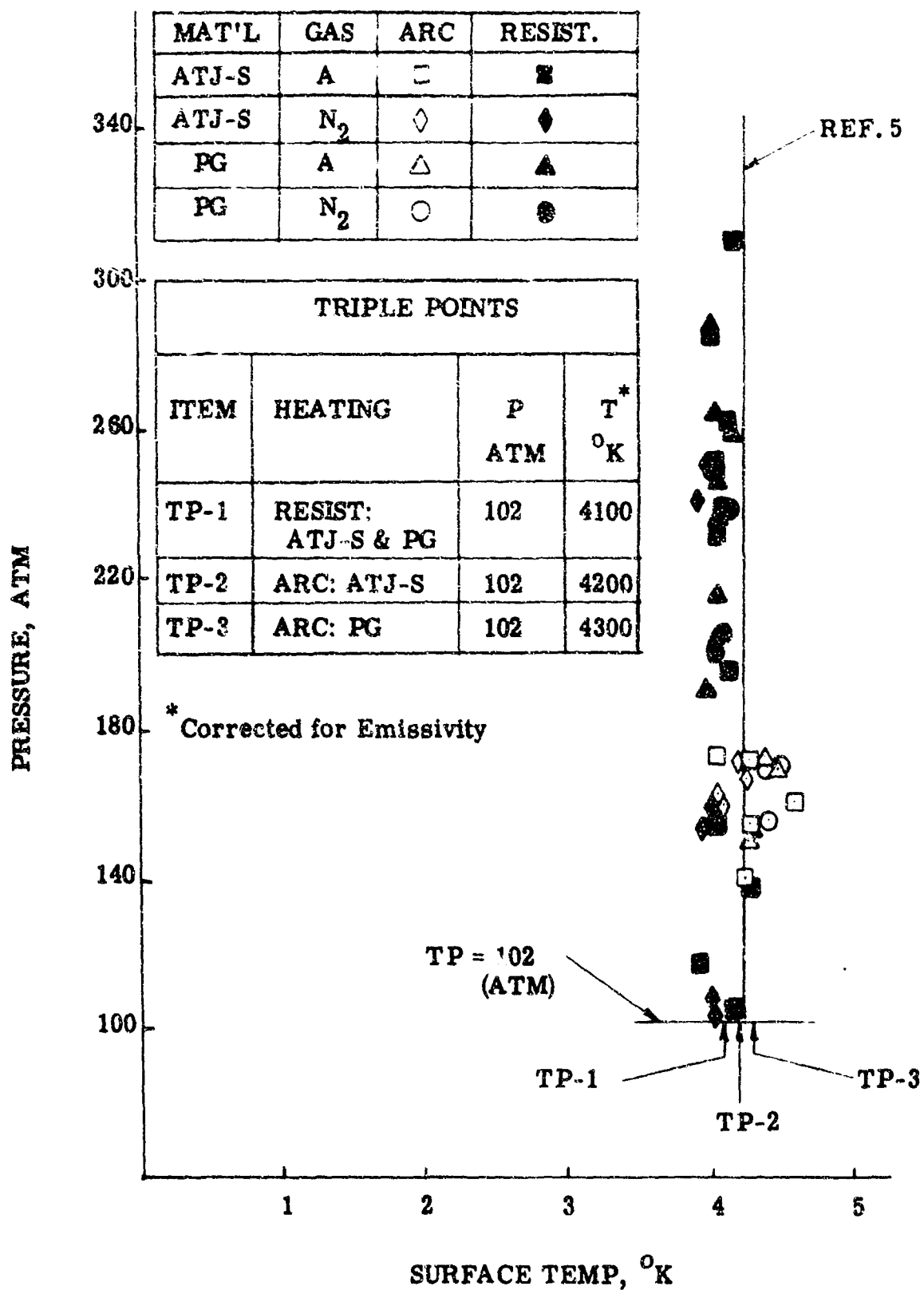


FIGURE 33. CORRECTED GRAPHITE PHASE DIAGRAM

TABLE I

CHEMICAL ANALYSES OF GRAPHITE MATERIALS

Material	Element (PPM)								
	Na	K	Ca	Fe	Al	Mg	Ti	Li	Ash
ATJ-S	7	0.8	8	*	*	1.4	*	<.5	334
ATJ (Purified)	3.0- 6.5	0.3- 0.6	1.1- 2.8	12- 74	1.6- 5.4	0.35- 5.6	0.5- 0.6	*	440
Pyrolytic Graphite	0.1- 1.3	0.1- 0.8	0.06- 4.7	1.0	0.01- 0.33	0.15- 6.0	1.0	*	10- 30

*Not Available

TABLE II
TEST DATA - ARC HEATING

Mat'l	Gas	Press. atm	Temp. °K	Temp. °K
ATJS	Argon		$\epsilon = 1.0$	$\epsilon = .89$
		174	3820	4055
		172	4050	4307
		161	4330	4614
		156	4040	4296
		141	4010	4263
ATJS	Nitrogen	172	3960	4208
		168	4020	4274
		163	3810	4044
		160	3860	4099
Pyrolytic Graphite	Argon		$\epsilon = 1.0$	$\epsilon = .7$
		173	3750	4371
		169	3840	4484
		154	3720	4334
		151	3680	4284
Pyrolytic Graphite	Nitrogen	171	3860	4506
		170	3800	4434
		157	3770	4396

TABLE III
TEST DATA - RESISTANCE HEATING

Mat'l	Gas	Press. atm	Temp. °K	Temp. °K
ATJS	Argon		$\epsilon = 1.0$	$\epsilon = .89$
		310	4090	4180
		285	3910	3992
		262	4050	4140
		252	3940	4023
		248	3950	4034
		238	4010	4096
		232	3960	4044
		196	4060	4148
		156	3960	4044
		138	4220	4316
ATJS	Nitrogen	118	3820	3898
		106	4080	4169
		251	3860	3940
		241	3830	3908
		204	3980	4064
		152	3930	4013
		154	3840	3919
Pyrolytic Graphite	Argon	108	3920	4002
		103	3970	4054
			$\epsilon = 1.0$	$\epsilon = .7$
		257	3780	4024
		264	3810	4058
		258	3920	4183
		247	3850	4104
Pyrolytic Graphite	Nitrogen	237	3820	4070
		216	3810	4058
		191	3720	3956
		238	3920	4183
		205	3870	4126
		201	3800	4047